THESIS

SUMMERTIME SPATIOTEMPORAL PATTERNS OF NITROGEN OXIDES (NO_X) IN SALT LAKE CITY

Submitted by

Daniela Carolina Guevara Proaño

Department of Atmospheric Science

In partial fulfillment of the requirements

For the Degree of Master of Science

Colorado State University

Fort Collins, Colorado

Fall 2025

Master's Committee:

Advisor: Emily V. Fischer

Jeffrey L. Collett, Jr
Shantanu Jathar

ABSTRACT

SUMMERTIME SPATIOTEMPORAL PATTERNS OF NITROGEN OXIDES (NO_X) IN SALT LAKE CITY

Salt Lake City, UT experiences persistent summertime ozone (O_3) exceedances of the National Ambient Air Quality Standard (NAAQS). During the 2024 Salt Lake City-Summer Ozone Study (SLC-SOS), we deployed the Aerodyne dual channel Cavity Attenuated Phase Shift Monitor (CAPS) in a mobile laboratory to quantify regional gradients and daily variability of nitrogen oxides (NO_x). Our analysis for smoke-free days include: (1) ambient NO_x abundances and NO_2/NO_x ratios from vehicle plumes compared with nearby urban cities; (2) regional NO_x gradients and morning-afternoon differences; and (3) weekday-weekend NO_x variability. Compared to other U.S. cities, NO_x abundances (7.7 ± 4.4 ppbv) and on-road NO_2/NO_x plume ratios (11.9 ± 10.3%) are higher than previously reported. Even after filtering near-vehicle emissions, there is a large east-west NO_x gradient in NO_x. The absolute value is methodologically dependent and varies from > 25 ppbv to ~4 – 5 ppbv. Maximum abundances are located at the Near Road (16.3 ppbv) and Utah Tech (11.7 ppbv) monitoring sites, and the minima are located at the Herriman #3 and Red Butte (< 3ppbv) monitoring sites. On weekday mornings, NO_x shows an east-west gradient of about a factor of ~10 between the Near Road and Herriman #3 sites, primarily driven by rush hour traffic. In the afternoon, the highest abundances shift southward, with gradients of ~11 to 50 ppbv (plume isolation method which removes short-lived NO_x peaks) under northwesterly winds. High-NO_x regions (e.g., Utah Tech, Rose Park, and Copper View) show stronger reduction of ~50 to 80% on weekends compared to low-NO_x western regions. These

results provide new insights into the spatiotemporal variability of NO_x in Salt Lake City to support the mitigation of high O_3 levels and improve air quality in the region.

ACKNOWLEDGEMENTS

I will be grateful with Emily all my life. Choosing you as my advisor has been the best decision I have ever made. With your energy, happiness, and passion for science, teaching, and mentoring, I have learned so many valuable lessons. Thanks for teaching me to think outside the box, to always question everything and ask the right questions, to communicate science properly, to stay curious and search for answers, and to always be patient and kind. Thank you for encouraging me to step out of my comfort zone to grow tremendously and teaching me that the main purpose of science is to serve people. I am deeply grateful for your support in the good but specially in the hardest moments. Thanks to you, today I am a better scientist and a better person. I am so happy to continue working and learning with you!

Thanks to my committee Jeff and Shantanu and the Fischer's research group, I'm confident I will continue improving my research with all your advice and feedback and growing as scientist. I am also very grateful to the CSU Dep. of Atmospheric Science for giving me this opportunity, for creating an inclusive and supportive environment, and helping me in countless ways.

Thanks to the incredible SLC-SOS and FROZÉ teams. I feel so fortunate to have learned from amazing scientists about teamwork, creative problem-solving, and how fun science is. I also extend my gratitude to Aerodyne Research Inc. for their support with the CAPS NO_x-NO_2 instrument, as well as all the science and data teams involved in the SLC-SOS project. I want to thank NOAA for supporting the 2024 mobile laboratory deployment in Salt Lake City, NCAR for helping us with the field catalog, NSF for funding this research, as well as the Fulbright Commission and Senescyt Ecuador for supporting my graduate studies.

To all my amazing friends I've made in the U.S., thanks for being family away from home. Thanks to Silvi and Gladys for their kindness and laughs; to Lena and Brandon for their endless support; to Delián for always reminding me to celebrate; and to all my Latin friends for reminding me how beautiful our cultures are! Thanks to Emi for being the best veci and friend, and for always being present and making us feel at home. Thanks to Juli for being one of my first mentors and inspire me to continue learning. I hope in the future we can work together to contribute to science and air quality in Ecuador. You have all made this experience so much more joyful! Y a todos mis amigos ecuatorianos, Ivonne, Majito, Patty, Fera, Esteban, Luchito y Jorge, gracias por quedarse cerquita siempre. Su lealtad, empuje y amor me han permitido sentirme siempre acompañada pese a la distancia.

Por último, un millón de gracias a mi familia. A mis papitos, Lupita y Javi, por todos los sacrificios que han hecho toda su vida por nuestra familia. Me enseñaron el valor del trabajo honesto, la generosidad, la humildad y el dar sin medida. A mi ñaña, mi compañera de vida, gracias por haber sido el apoyo más grande, el mejor equipo y nunca dejarme caer. Todo esto fue más maravilloso junto a ti. A mi ñaño y Majito, por siempre inspirarme con su ejemplo y motivarme a soñar en grande. A mi sobris Ame, por recordarme que siempre hay tiempo para jugar. A mis perritos Benji y Lulú, por no olvidarse de mí. Y a mi tía Michita y abuelita Amelita por haber sido mis segundas madres. A todos ustedes familia, gracias por querer verme feliz siempre, haberme enseñado a confiar en mi potencial y por su amor incondicional. Este logro es gracias a ustedes. ¡Los amo!

Todavía hay tanto que quiero aprender, hacer, ser y dar. Este es un nuevo comienzo.

¡Ser más, para servir mejor!

DEDICATION

To my grandma Amelia and my uncle Byron, whom I lost over the past two years.

Thanks for reminding me that wherever I go and whatever I do,
I should always remember where I come from.

TABLE OF CONTENTS

CHAPTER 1 : INTRODUCTION

Ozone (O_3) is a secondary pollutant responsible for major health effects including causing and worsening asthma, chronic bronchitis (Nuvolone et al., 2018; Tilton, 1989; US EPA, 2015a), cardiovascular disease, and increases in premature mortality (Nuvolone et al., 2018). Furthermore, O_3 damages natural vegetation and reduces crop yields (Emberson, 2020; McGrath et al., 2015; US EPA, 2015b) across the United States (Erickson et al., 2020). The interactions between O_3 and vegetation can also impact local and regional climate since O_3 uptake through plant stomata reduces plant photosynthesis and stomatal conductance which influences evapotranspiration across land surface ecosystems (Zhou et al., 2024) and O_3 is also a potent greenhouse gas (Shindell et al., 2006).

Nitrogen oxides ($NO_x = NO + NO_2$), which include nitric oxide (NO) and nitrogen dioxide (NO_2), are critical precursors for ground-level O_3 formation (Logan, 1983). O_3 is produced when volatile organic compounds (VOCs) are oxidized in the presence of NO_x (Blaszczak-Boxe et al., 2025; Erickson et al., 2020). NO can also remove O_3 by titration, making NO_x both a major precursor and a regulator of urban O_3 levels (Jhun et al., 2015). The U.S. Environmental Protection Agency (EPA) regulates ground-level O_3 under the National Ambient Air Quality Standards (NAAQS), with the current standard set at 70 parts per billion (ppb) for the 3-year average of the 4th highest daily 8-hour average concentration (US EPA, 2025). This threshold was lowered from 75 ppb in 2015 to strengthen protection for sensitive populations (McCarthy & Shouse, 2015). Areas where monitored values exceed the NAAQS are designated as nonattainment, and this designation triggers a series of regulatory actions. Although this regulatory framework has driven significant reductions in O_3 over past decades over much of the U.S., several challenges remain in the western U.S. (Chang et al., 2025; Cooper et al., 2015).

In addition to its role as direct O_3 precursor, NO_2 is also a criteria air pollutant. The NAAQS for NO_2 is 100 ppb for a 1-hour average concentration (US EPA, 2025). Exposure to NO_2 is not evenly distributed in the U.S.; some minoritized populations (e.g., Blacks/African Americans, Hispanics, Asians, and others) and people of low socioeconomic status often experience much higher exposures due to proximity to major highways and emission sources (Clark et al., 2014; Wang et al., 2023). There is also evidence that this pollutant is harmful to children at levels below the standard; health effects of concern include exacerbation of asthma, decreased cognitive and neurological function, and even poorer academic performance, since children spend much of their time at school, where elevated pollutant levels can significantly contribute to their total exposure (Bechle et al., 2023; Zetlen et al., 2025).

According to the 2020 National Emissions Inventory (NEI), NO_x emissions in the U.S. (Figure 1) predominantly originate from anthropogenic combustion processes, particularly on-road mobile emissions, with heavy-duty diesel vehicles accounting for the largest emissions (Ma et al., 2024). Stationary sources such as power plants and industrial facilities also contribute significantly, while natural sources including lightning and soil emissions have a smaller contribution in urban environments compared to fossil fuel combustion (US EPA, 2020). NO_x distributions in urban areas show strong spatial gradients, with the highest concentrations typically occurring near major roadways (Richmond-Bryant et al., 2017). There is also a seasonal and diurnal variability, with concentrations generally lower in summer than in winter due to the combined effects of increased mixing and dispersion, reduced vehicle emissions on warmer days, and increased NO_x emission controls on power plants during summer (Duncan et al., 2010; Lamsal et al., 2010). Over the past two decades, NO_x emissions have declined substantially in the U.S. as a result of more regulation programs implemented on vehicles and power plants, including the

NO_x SIP Call, the Cross-State Air Pollution Rule (CSAPR), and the Tier 3 Light-duty Vehicle Emissions and Fuel Standards (US EPA, 2015c); however, recent evidence indicates that this trend is slowing down in some regions (Dix et al., 2020; Goldberg et al., 2021). Therefore, continued attention from both research and policy communities is needed to continue to mitigate the adverse impacts of NO_x on air quality and public health.

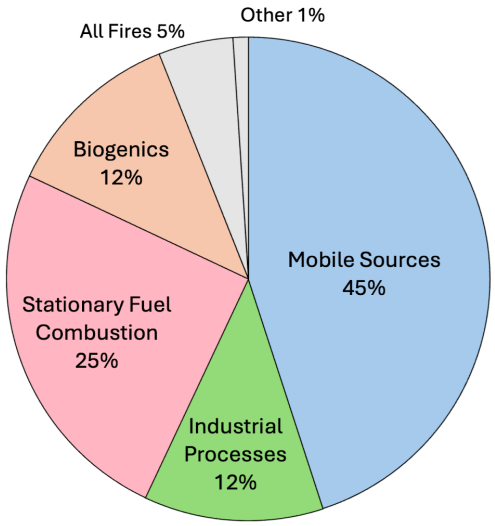

Figure 1. U.S. NO_x emissions by sector. Source: NEI, 2020.

One key motivation for this work is that the abundance and spatiotemporal gradients of NO_x have important implications for O_3 formation in and downwind of urban airsheds. NO_x emissions lead to elevated concentrations that strongly influence local O_3 photochemistry (Lu et al., 2019) and shape local and regional O_3 distributions (Fishman et al., 1979; Logan, 1983). The response of O_3 to these emissions is nonlinear and regulatory discussions often center on identifying locations that fall into one of two production regimes: NO_x-limited, where additional NO_x enhances O_3 formation, and VOC-limited regime (NO_x-saturated), where excess NO_x suppresses O_3 production through radical scavering and titration (Donzelli & Suarez-Varela, 2024; Duncan et al., 2010). In the U.S., NO_x emissions reductions have shifted many urban cores from VOC-limited toward NO_x-limited conditions (Koplitz et al., 2021). In addition to this chemical complexity, there

are strong spatial gradients and temporal patterns, such as elevated NO_x during rush hours, weekday-weekend differences, and seasonal contrasts that also influence O_3 production and challenge air quality management (Donzelli & Suarez-Varela, 2024; Lu et al., 2019).

Salt Lake City (SLC), located in the Northern Wasatch Front of Utah, has a population of nearly 3 million residents (Bureau, 2025) and is designated as a non-attainment area for the 2015 for 8-hour O_3 standard (EPA, 2015). High O_3 mixing ratios are a persistent summertime concern in the region, where exceedances of the 70 ppb NAAQS have occurred during multiple recent seasons, sometimes on more than 30 days per summer (Jaffe et al., 2018). This is driven by a combination of local photochemistry (Monks et al., 2015), complex terrain circulations that trap pollutants (Horel et al., 2016), and smoke injections from local wildfires and wildfires located across upwind regions of the western U.S. The presence of wildfire smoke elevates both O_3 and particulate matter in this area (Jaffe & Wigder, 2012). Previous work has used short term intensive field studies and observations from the extensive regulatory network to quantify how lake-breeze circulations (Blaylock et al., 2017), TRAX light rail car emissions (Mendoza et al., 2019), and vehicle combustion efficiency (Yañez et al., 2025) contribute to the O_3 problem in Salt Lake City. Early studies, such as the 2015 Great Salt Lake Summer Ozone Study ($GSLSO_3S$), show that high O_3 events can be due to both dynamics (strong ridging) and the presence of wildfire smoke, but these studies did not focus on the abundance or distribution of O_3 precursors. More recently, the 2022 Salt Lake Regional Smoke, Ozone, and Aerosol Study (SAMOZA), began to address this gap by adding additional measurements of VOCs, CO, O_3, and carbonyl species at the Utah Technical Center monitoring site. This augmented ongoing regulatory measurements of O_3, CO, NO_x, and $PM_{2.5}$ at this location. The analysis of this combined dataset thus far has demonstrated that O_3 production in SLC is VOC-limited at this site and highly responsive to the presence of

wildfire smoke (Cope et al., 2024; Ninneman et al., 2023). Another study, which used 2019-2021 data, indicates there appears to be a limited O_3 sensitivity to changes in NO_x at Hawthorne monitoring site associated with the ~60% NO_x reductions since 2000, and large weekday-weekend differences in NO_x emissions (~20%). There is however still much we do not know about O_3 and its precursors in this area, limiting the development of effective mitigation strategies.

The Salt Lake City Summer Ozone Study 2024 (SLC-SOS 2024) was conducted in August 2024 and included the deployment of the Wyoming Mobile Research Lab (UW Lab) to measure O_3 and its precursors across the Salt Lake Valley. This project aims to advance understanding of O_3 chemistry, provide spatiotemporal gradients, characterize precursor sources, evaluate wildfire smoke impacts, and reduce uncertainties in emissions inventories. Within this framework, we focus specifically on the summertime spatiotemporal patterns of NO_x in Salt Lake City. Although urban NO_x emissions in U.S. cities have declined by 30% - 70% between 2005 and 2019 (Goldberg et al., 2021), Salt Lake City continues to experience elevated NO_x from traffic, industry, and basin meteorology that traps pollutants. Although NO_2 concentrations have decreased since 2000 across most monitoring sites, annual averages remain between 10 - 20 ppbv since 2012. According to the 2020 NEI, mobile sources account for approximately 74% of total NO_x emissions in Salt Lake and Davis counties, with the largest mobile contributions from on-road diesel heavy-duty vehicles (34%) and non-diesel light-duty vehicles (27%) (Figure 2). The spatiotemporal variability of NO_x remains a key uncertainty in O_3 predictions, and substantial reductions are still required to meet the standards in this area (Cope et al., 2024; Ninneman et al., 2023).

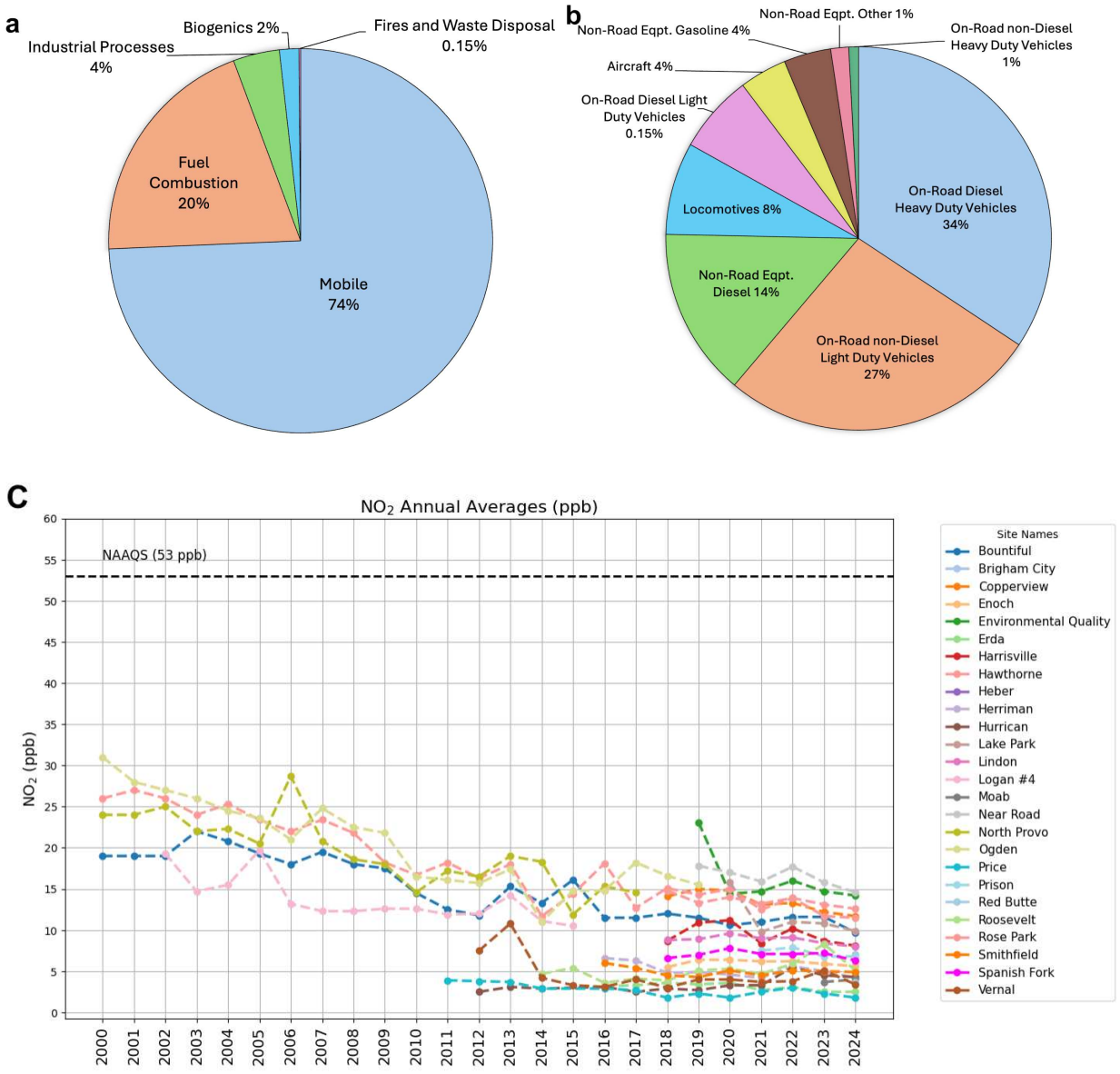

Figure 2. Distribution of NO_x emissions for Salt Lake and Davis counties. (a) Total NO_x emissions by major sector; (b) mobile-source NO_x emissions by vehicle and equipment type; and (c) NO_2 annual average trends and comparison to NAAQS for NO_2 during the period 2000-2004. Source: .

This study provides a better understanding of summertime NO_x abundances and distributions across SLC using mobile measurements from the 2024 SLC-SOS field campaign and stationary observations from the Utah Department of Air Quality (DAQ) monitoring network. We hypothesize that summertime NO_x in SLC exhibits a strong spatial and temporal variability, driven

primarily by vehicle emissions, with higher abundances during weekdays than weekends. To test these hypotheses, the goals of this work are to (1) characterize NO_2/NO_x ratios of vehicle exhaust plumes and ambient NO_x abundances; (2) quantify the spatiotemporal variability of summertime NO_x concentrations; and (3) investigate differences in NO_x emissions patterns between weekdays and weekends. To address these goals, we first identify smoke-impacted days using a satellite-based smoke plume product with surface $PM_{2.5}$ and CO measurements because wildfire smoke enhances O_3 concentrations, especially in urban areas with high NO_x concentrations (Brey & Fischer, 2016a; Jaffe et al., 2024; Ninneman et al., 2023). Given the goal of supporting effective policy to reduce O_3, our analysis then focuses primarily on smoke-free conditions. Then, we isolate fresh vehicle plumes with a plume detection algorithm adapted from previous studies and calculate NO_2/NO_x ratios for plumes. We quantify ambient abundances of NO_x, CO, and CO_2 by applying established filtering methods to remove local exhaust plumes from mobile measurements. Finally, we present the spatial and temporal variability of NO_x across the region, including regional gradients, diurnal patterns, weekday morning versus afternoon differences, and weekday versus weekend contrasts.

CHAPTER 2 : METHODS

2.1 Instrumentation and Measurement Details

2.1.1 SLC-SOS 2024 Experimental Design

The 2024 Salt Lake City Summer Ozone Study (SLC-SOS) was conducted from 1 August to 30 August 2024 (Figure A1) along the Wasatch Front in northern Utah. Mobile observations were performed using the Wyoming Mobile Research Lab (UW Lab), equipped with six different instruments for measuring O_3 and its precursors and meteorological parameters (Table 1, Figure A2). In coordination with the University of Utah and NOAA, the team-based drive plans off daily forecasts. We conducted 24 daytime drives during both weekday-weekend and morning-afternoon periods, and the UW Lab was stationary at the Mountain Met Building (MMB) also known as the Red Butte UDAQ Monitoring Site (40.76643, -111.82822) for 10 periods. Drive routes (Figure 3) were directly linked to the project research goals related to either O_3, NO_x, CH_4, or VOC sources.

The main gas analyzers, including the CAPS NO_x-NO_2, ROZE O_3, Picarro G2401-m, and Aeris MIRA ethane/methane instruments were connected to a shared sampling line with separate tap-offs with a total combined flow of ~9.6 LPM. The PTR-ToF-MS was on a separate inlet to reduce inlet residence time. Each instrument is described below, with more attention given to the focus of this thesis and to instruments without prior deployment.

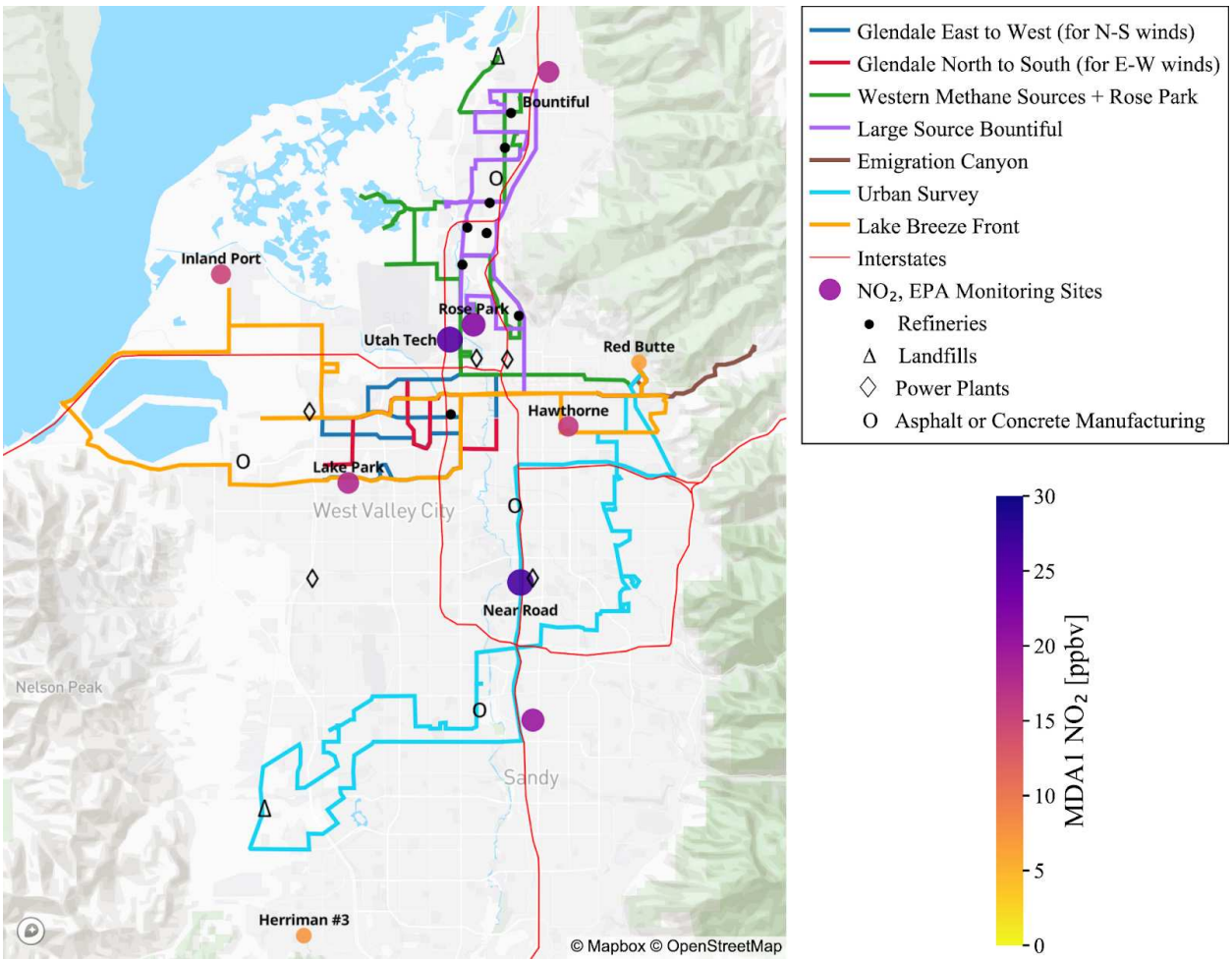

Figure 3. Map of SLC-SOS drive routes, point emission sources, and monitoring sites. The colored lines represent the planned drive routes, black dots denote the refinery sites, triangles indicate the landfill sites, diamonds represent power plants, and circles denote asphalt or concrete manufacturing. Colored circles represent EPA monitoring sites, with both color and size indicating median daily maximum 1-hour average NO_2 concentrations (MDA1) for the 2019-2024 period (June-September).

Instrument	Species Measured	Reference
Aerodyne Cavity Attenuated Phase Shift (CAPS NO_x)	NO_x($NO + NO_2$)	(Kebabian et al., 2008)
Ionicon Proton Transfer Reaction Mass Spectrometer (PTR-MS)	Speciated VOCs	(X. Wang et al., 2021)
Rapid OZone Experiment (ROZE) UV Absorption Instrument	O_3	(Hannun et al., 2020)

Mid-IR Absorption Spectroscopy / AERIS MIRA Ultra Series Mobile Analyzer	C_2H_6, CH_4	(Commane et al., 2023)
MIRO MGA-10 GP Multi Compound Gas Analyzer	CO, CO_2, CH_4, H_2O, O_3, NO, NO_2, NH_3, SO_2, OCS	(Tillmann et al., 2022)
Picarro Cavity Ring Down Spectroscopy (Model G2401-m) Analyzer	CO_2, CO, CH_4, H_2O	(Commane et al., 2023; Mouat et al., 2024)
UW Sprinter Van Monitoring System (AIO)	Wind, RH, T, P, and GPS R100	-

Table 1. Overview of UW Lab payload for the 2024 SLC-SOS deployment.

2.1.1.1 NO_x, NO_2, and NO Measurements

The Aerodyne Research dual-channel Cavity Attenuated Phase Shift oxides of nitrogen (CAPS NO_x) monitor measures ambient NO_x and NO_2 (Kebabian et al., 2005, 2008) (Figure A3, A4, and A5). The instrument provides a direct measurement of NO_2 via optical absorption at 450 nm using a blue light-emitting diode (LED) within a high reflectivity optical cavity. NO is converted to NO_2 by the reaction with photolytically produced O_3 and thus NO_x is measured as NO_2. NO is then determined by the difference of the NO_x and NO_2 measurements. For this deployment, we operated at a sample flow rate of 1.2 SLPM per channel (2.4 SLPM total). Pre campaign tests with a filtered inlet indicate that this results in a signal recovery time of approximately 4-5 seconds per channel. NO and NO_2 measurements were recorded at a frequency of 1 Hz. The 1-Hz detection limits (3σ noise) were 0.36 ppbv for NO_2, 0.61 for NO_x, and 0.70 ppbv for NO and accuracy is ±10% of the measured mixing ratios (Appendix IV, Section A).

We are the first users of the Aerodyne dual channel CAPS NO_x-NO_2 Monitor, and this is the first deployment in a field campaign. Overall, we had a good performance and stability over the field campaign (see calibration summary below). However, after the first test drive in SLC, the lamp used to photolytically produce O_3 failed, so we were only able to measure NO_2 during Drive 2 for the Emigration Canyon route. All subsequent drives were completed without further technical difficulties.

Pre-deployment calibrations were performed in the laboratory, during the installation in the mobile laboratory in Laramie, WY, and ahead of test drives in Salt Lake City, UT. During the field campaign, calibrations were performed on the ground between drives approximately one time per week. Post-campaign calibrations, that included a cross check of the primary standards, were performed in the laboratory after the field campaign. Prior and after each calibration, ultra zero air (UZA) gas was flushed through the inlet for five minutes. Then, the instrument was calibrated with diluted mixtures of NO or NO_2 from certified cylinders of 1.07 ± 0.10 ppm NO in N_2 (Linde Gas #CB10671, certification date: 4/10/2024) and 1.164 ± 0.116 ppm NO_2 (Airgas #EA0033295, analysis date: 03/13/2024) in UZA. Each calibration consisted of a five-point linear dilution curve ranging from 400 to 50 ppbv. After the field campaign, we calculated the slope and the standard deviation of each calibration curve using a Linear Least Squares (LLS) fit (Figures A6, A7, and A8).

2.1.1.2 O_3 Measurements

O_3 was measured using the NASA Rapid Ozone Experiment (ROZE), an instrument that utilizes UV-based incoherent broadband cavity enhanced absorption spectroscopy (Hannun et al., 2020). For this deployment, ROZE was operated at ambient pressure using its internal linear diaphragm pump, maintaining a flow rate of approximately 10 LPM in the mobile laboratory. The

instrument provided high time resolution data at 1Hz, and a 15-second data gap occurs every 15 minutes due to the instrument's automatic zeroing routine, in which sample air is passed through a MnO_2 scrubber to remove any ambient O_3. ROZE was calibrated on non-drive days by using the Rayleigh attenuation as a function of pressure in O_3-free air, as the instrument is sensitive to Rayleigh scatter. The measurement uncertainty is estimated at ± 6.2% (1σ), based on previous characterizations and field deployments. In general, the instrument maintained stable accuracy throughout the field campaign, with no significant interferences identified. Concentrations observed ranged from levels below 5 ppbv during early morning drives to values exceeding 80 ppbv during afternoon drives.

2.1.1.3 CO and CO_2 Measurements

Carbon monoxide (CO) and carbon dioxide (CO_2) were measured using the UWPicarro G2401-m analyzer, which uses closed path cavity ring-down spectroscopy (CRDS) (Crosson, 2008). For this deployment, the instrument was operated at 45°C and 140 Torr, with a flow rate of 600 mL/min. The ultra-high reflective mirrors enable multiple passes in the cavity creating an effective path length greater than 10 km, resulting in high sensitivity (Crosson, 2008). Precision under field conditions is approximately ± 30 ppb for CO and ± 200 ppb for CO_2. The analyzer recorded data at a reporting rate of ~0.5 Hz, and H_2O measurements were used for automatic correction to dry gas mole fraction. Calibrations during the deployment were performed using high precision NOAA ESRL-traceable standards and zero checks were conducted periodically using ultra zero air (UZA) gas.

2.1.2 Stationary Measurements

The Utah Division of Environmental Quality Division of Air Quality (Utah DEQ-DAQ) operates a monitoring network across the state with 23 sites measuring $PM_{2.5}$, 22 sites measuring

O_3, 21 sites measuring NO, NO_2, and NO_x, and 7 sites monitoring CO. Each site also includes measurements of meteorological parameters including ambient temperature (T_{amb}), relative humidity (RH), solar radiation (SR), and wind speed and direction. For this study, we used observations from ten monitoring sites within the Salt Lake Valley that overlapped with the SLC-SOS mobile drive routes: Bountiful Viewmont, Inland Port, Rose Park, Utah Technical Center, Hawthorne, Lake Park, Near Road, Copper View, Herriman #3, and Red Butte (MMB where the UWyom van was parked). Table 2 provides a summary of the selected monitoring sites, their location type, and species measured. This data was obtained from EPA Air Data (https://www.epa.gov/outdoor-air-quality-data). UDAQ reports UTC hourly average concentrations using Federal Equivalent Methods (FEMs), including ultraviolet (UV) absorption for O_3 (Teledyne API T400), gas phase chemiluminescence for NO_x, NO_2, and NO (Teledyne API T200U), and a beta-attenuation instrument for $PM_{2.5}$ (Thermo 5030i Sharp). Meteorological variables are recorded using electronic thin film or resistance sensors for temperature and humidity, and pyranometers for solar radiation as detailed in the Annual Monitoring Network Plan 2024 (UDEQ, 2024). Station data undergo regular validation based on two-week quality control (QC) checks, including zero/span verifications and flow rate measurements. Post-processing includes flagging outliers and ensuring compliance with the NAAQS as it is detailed in the Quality Assurance Project Plan (QAPP).

DAQ Monitoring Site	Location type	Species measured
Bountiful Viewmont	Suburban, refineries area	BP, CO, NO, NO_2, NO_x, O_3, RH, $PM_{2.5}$, PM_{10}, SO_2, wind speed and direction, and T
Inland Port	Industrial, vehicular area	$PM_{2.5}$, O_3, NO, NO_2, NO_x, wind speed and direction, T, and ceilometer

Rose Park	Minority neighborhood, vehicular, refineries area	CO, O_3, NO, NO_2, NO_x, $PM_{2.5}$, PM_{10}, SO_2, wind speed and direction, T, and ceilometer
Utah Technical Center	Suburban, industrial, airport area	CO, O_3, NO, NO_2, NO_x, $PM_{2.5}$, PM_{10}, SO_2, wind speed and direction, T, and ceilometer
Hawthorne	Neighborhood urban area	CO, NO, NO_2, NO_x, NO_y, O_3, $PM_{2.5}$, PM_{10}, rainfall, RH, SO_2, SR, wind speed and direction, T, ceilometer, and gas chromatograph
Lake Park	Suburban, Great Salt Lake, port area	$PM_{2.5}$, O_3, NO, NO_2, NO_x, wind speed and direction, and T
Near Road	Vehicular traffic area	CO, O_3, NO, NO_2, NO_x, RH, wind speed and direction, T, and SR
Copper View	Suburban vehicular area	CO, O_3, NO, NO_2, NO_x, $PM_{2.5}$, RH, SO_2, SR, T, wind speed and direction
Herriman #3	Suburban neighborhood	O_3, NO, NO_2, NO_x, $PM_{2.5}$, PM_{10}, wind speed and direction, and T
Red Butte	MMB, University of Utah	O_3, NO, NO_2, NO_x, NO_Y, NO & Diff., $PM_{2.5}$, wind speed and direction, T, and ceilometer

Table 2. Summary of selected DAQ monitoring sites including their location and species measured. Abbreviations: BP = barometric pressure, RH = relative humidity, SR = solar radiation, and T = temperature.

2.2 Data Processing

2.2.1 Traffic-Filtering

Traffic-related NO emissions can titrate O_3 through fast chemical reactions ($NO + O_3 \rightarrow NO_2 + O_2$), leading to low O_3 values that coincide with elevated NO concentrations in freshly emitted plumes (Wild et al., 2017). Therefore, filtering direct emissions from nearby vehicles is essential to building a more regionally representative picture of ambient NO_x and O_3 based on mobile monitoring measurements. In this study, NO (CAPS NO_x-NO_2) measurements were time-aligned with corresponding CO_2 (Picarro), and O_3 (ROZE) data by applying variable time

offsets based on peak matching. Then, two published filtering methods, as described in the following sections, were used to either calculate regionally representative levels (i.e., by removing the influence of vehicles directly in front of the mobile lab) or to isolate individual plumes of vehicle emissions for analysis of emission ratios.

2.2.1.1 Estimating background levels using SIBaR method

The SIBaR (State-Informed Background Removal) method uses a hidden Markov model (HMM) framework to identify background and near source-influenced periods, assigning each measurement to a lower or higher concentration state by detecting regime changes in the time series (Actkinson et al., 2021). The HMM identifies "chains" or sequences of similar measurements, classifying them into state sequences which are determined by maximizing a log-normal likelihood function that best represents the probability distribution of the observations. In this application, the word background applies to mobile measurements that have been filtered to remove local plumes likely associated with vehicles in close proximity to the mobile laboratory. We used the SIBaR method to identify background levels or non-hyper-local plumes of NO_x, CO, and CO_2 that still have an urban/anthropogenic influence. The method was applied to each drive individually, using the publicly available code. Figure 4 shows two examples of the application of the SIBaR method for O_3 and NO_x. When applied to the data collected during Drive 8, conducted during the afternoon under expected lake breeze flow, the method successfully removes the high NO_x concentrations associated with direct emissions. In contrast, when this method was initially applied to the data collected during Drive 14, which was an urban survey conducted in the early morning, SIBaR classified a location with regionally elevated NO_x sampled between 7:17 - 8:37 AM as a near source-influenced period. To address this, we reapplied SIBaR to shortener chunks of data within these periods, which allowed us to better distinguish the regionally elevated NO_x

from the nearest local sources. This was repeated across most of the early morning drives where the same pattern was observed.

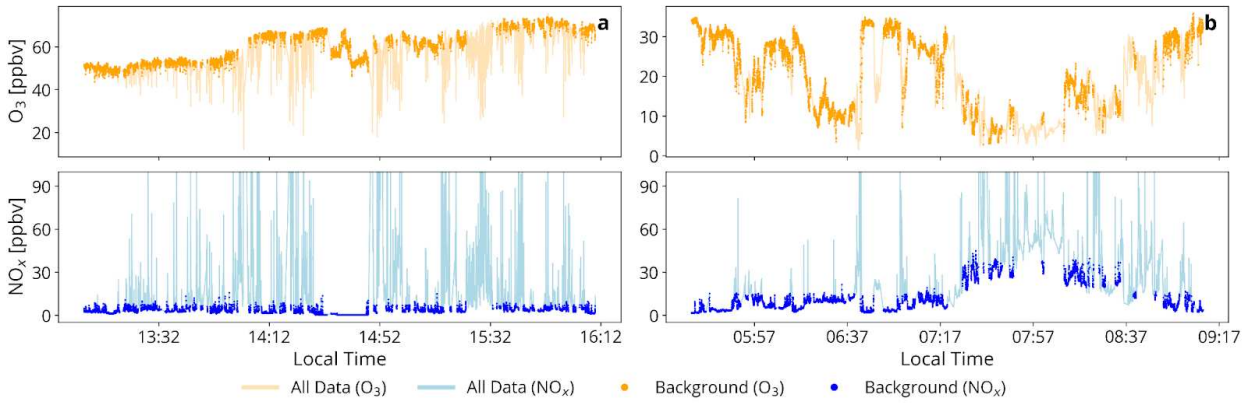

Figure 4. Examples of O_3 and NO_x data background using the SIBaR method (timestamps shown in Mountain Time) for (a) Drive 8, Lake Breeze (6 August 2024), and (b) Drive 14, Urban Survey (16 August 2024).

2.2.1.2 Plume isolation method

To isolate vehicle exhaust plume events, we applied a plume-by-plume detection algorithm adapted from Wild et al. (2017) and Zuraski et al. (2025), with modifications for Salt Lake City conditions. Prior to the plume detection, we excluded NO, NO_2, and NO_x values exceeding 1000 ppbv, based on the measurement range of the CAPS instrument. Plumes were defined as short duration NO_x concentrations spikes, with the start identified when the time derivative of NO_x exceeded 20 ppbv/s. This threshold better captured plumes sampled in Salt Lake City compared to the 25-30 ppbv/s values used in previous studies for other US cities. We chose to use the lower threshold (i.e., 20 ppbv/s) because the higher thresholds did not fully capture coincident periods of O_3 titration. Then, the end of each plume was defined when NO_x values returned to within 20 ppbv of their initial concentration. To better define non-plume levels for regression analysis, two seconds were added before and after each plume (Figure A9). An example of this method applied to Drive 8 for the Lake Breeze route is shown in Figure 5a, where NO_x spikes and O_3 titration indicate plume periods. The same time intervals identified as NO_x plumes were also removed from

the corresponding O_3 data. This method was applied to each of the 19 smoke-free drive files individually, resulting in the identification of 878 NO_x plumes.

2.2.1.3 NO_2/NO_x ratio using the Total Oxidant Approach

We applied the total oxidant approach based on the methodology from Wild et al. (2017) and Zuraski et al., (2025) to determine the NO_2/NO_x ratio. For each plume identified with the plume-by-plume algorithm, we calculated the total oxidant (O_x) as the sum of O_3 and NO_2, then used a linear regression between O_x and NO_x for each plume containing more than three valid observations, and the slope of this fit is taken as the NO_2/NO_x ratio (Figure A9). Although Zuraski et al., (2025) included negative values, we limited our analysis to positive ratios, excluding the negative values did not significantly affect the results (Figure A10, Table A1). This method relies on several key assumptions: (1) O_3 is not directly emitted from vehicular exhaust; (2) the fast conversion of NO plus O_3 is conserved within the O_x/NO_x ratio, (3) NO_2 photolysis is conserved in the NO_x measurement over the short duration of each plume, and (4) the O_x/NO_x slopes are independent of the background levels which are assumed to remain constant within the duration of the plume. Figure 5b and 5c illustrate an example plume from Drive 8 (highlighted by the red box in Figure 3a), showing the individual mixing ratios of NO, NO_2, NO_x, O_3, and O_x and Figure 5d shows the linear regression and slope used to calculate the NO_2/NO_x ratio. Summary statistics including the arithmetic and geometric mean, median, and histogram peak, as well as a comparison with values reported for other cities are presented later in the results.

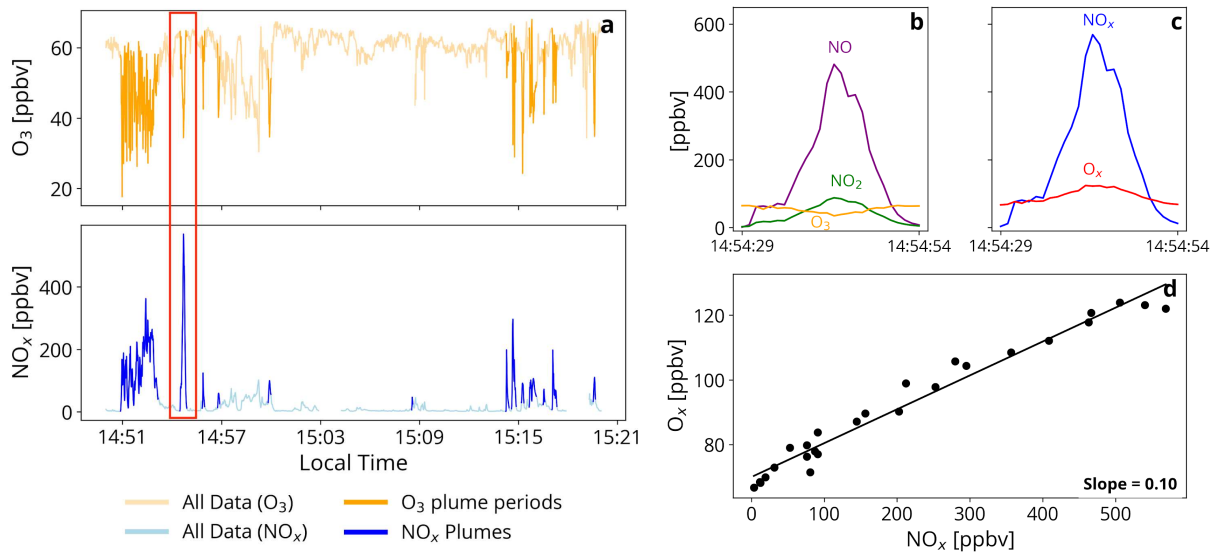

Figure 5. Example of a NO_x plume observed during Drive 8 for the Lake Breeze route. (a) Time series of O_3 and NO_x with plume periods highlighted; the red box indicates the selected plume analyzed. (b) Expanded view of the selected plume showing NO (purple), NO_2 (green), and O_3 (orange) mixing ratios. (c) O_x (red) and NO_x (blue) mixing ratios for the selected plume. (d) Correlation between O_x and NO_x during the plume period.

2.2.2 Wildfire Smoke Identification

Ground-level smoke-impacted days were identified with criteria used in previous studies (Brey & Fischer, 2016; Cope et al., 2024; Jaffe et al., 2024; Ninneman et al., 2023). Briefly, we combined surface-level $PM_{2.5}$ concentrations and smoke plumes from the NOAA Hazard Mapping System (HMS) (Kaulfus et al., 2017). A day was classified as smoke-impacted if: (1) the area was under a HMS smoke plume polygon, and (2) the daily average $PM_{2.5}$ concentration across UDAQ monitoring sites exceeded the August $PM_{2.5}$ mean + 1 SD of data collected during days without HMS smoke plumes overhead (i.e., smoke-free days) for all sites (6.90 µg/m^3). The use of both criteria is important, as the presence of an HMS plume does not guarantee smoke is present at the surface. Based on this method, a total of 11 days in August 2024 were classified as smoke-impacted (marked with black circles in Figure 6). Therefore, 5 of the 24 mobile drives were classified smoke-impacted, while the remaining 19 were considered smoke-free. There were two days (2 and 30 August) which showed high $PM_{2.5}$, but no HMS smoke overhead, and therefore were also

classified as smoke-free drives. The high $PM_{2.5}$ on those two days may originate from other local sources. We also considered CO measurements collected on the UW Lab in this analysis (stationary measurements of CO at DEQ sites have a low precision and their use is not recommended for mixing ratios < 400 ppbv). Even though CO is particularly sensitive to local traffic emissions, the largest smoke impacted periods (7-9 August and 24-25 August) are also characterized by elevated minimum CO. There is no CO data available for the last days of August because the field campaign concluded on 28 August, and the mobile measurements ended prior to that date.

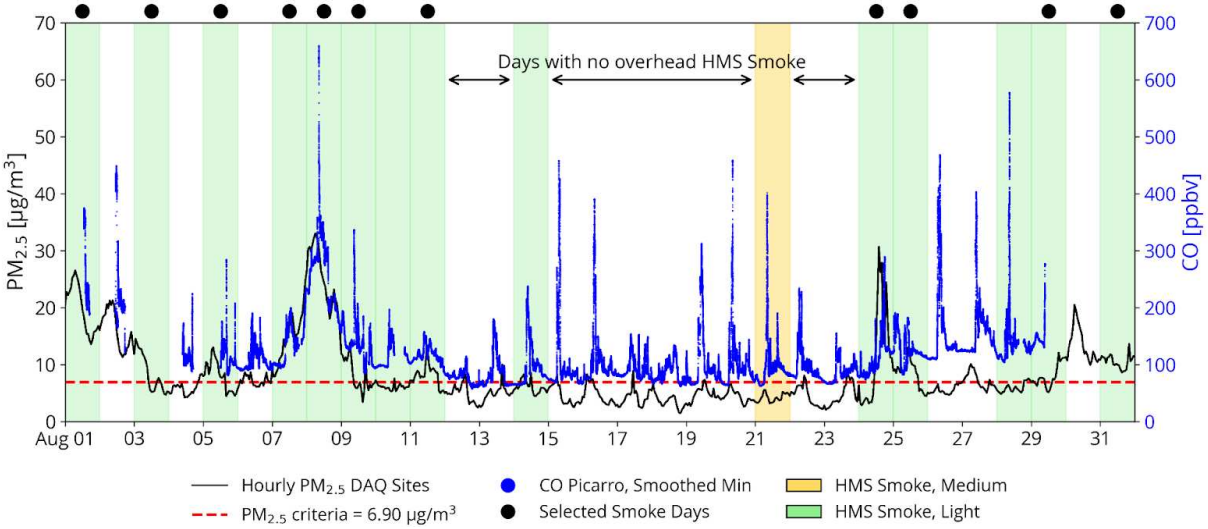

Figure 6. Time series of hourly $PM_{2.5}$ concentrations from DAQ monitoring sites and CO mixing ratios from UW Lab Picarro during August 2024. The dashed red line indicates the August $PM_{2.5}$ mean + 1 SD of smoke-free days for all sites (6.90 µg/m^3). Shaded regions denote days with overhead smoke identified by the NOAA HMS product: green for light smoke and yellow for medium smoke. Red circles at the top show selected smoke-impacted days.

2.3 Overview of Data Analysis

Our analysis begins with an overview of sampling conditions and O_3 abundances across ten DAQ monitoring sites. Focusing only on smoke-free drives, we quantify ambient levels of NO_x, CO_2, and CO in Salt Lake City using the SIBaR method and compare them to previous mobile measurements in Las Vegas and Los Angeles. Using the total oxidant approach, we

determine the NO_2/NO_x ratios from individual vehicle plumes and values observed for Salt Lake City in August 2025 with prior measurements from other western U.S. and international cities. We present regional NO_x maps using three filtering approaches (i.e., unfiltered, plume isolation, and SIBaR method) and quantify differences in abundance across the diurnal cycle by comparing observations collected during weekday morning and afternoon drives with diurnal profiles observed at DAQ monitoring sites. Finally, we examine the weekday-weekend differences in NO_x using both mobile measurements and stationary observations.

CHAPTER 3 : RESULTS

3.1 Overview of Sampling Conditions

During August 2024, O_3 mixing ratios across the ten DAQ monitoring sites showed notable daily variability (Figure 7). Elevated O_3 levels were generally observed at the beginning and end of the month during both smoke-free (white circles) and smoke-impacted days (black circles). In total, there were 7 days when O_3 levels exceeded the max daily 8-hour (MDA8) NAAQS value of 70 ppbv, with 5 drive-days classified as smoke-impacted and 13 as smoke-free. These patterns, illustrated in Figure 7, reflect the regional nature of high O_3 events in Salt Lake City, and that these events occur with and without the presence of wildfire smoke.

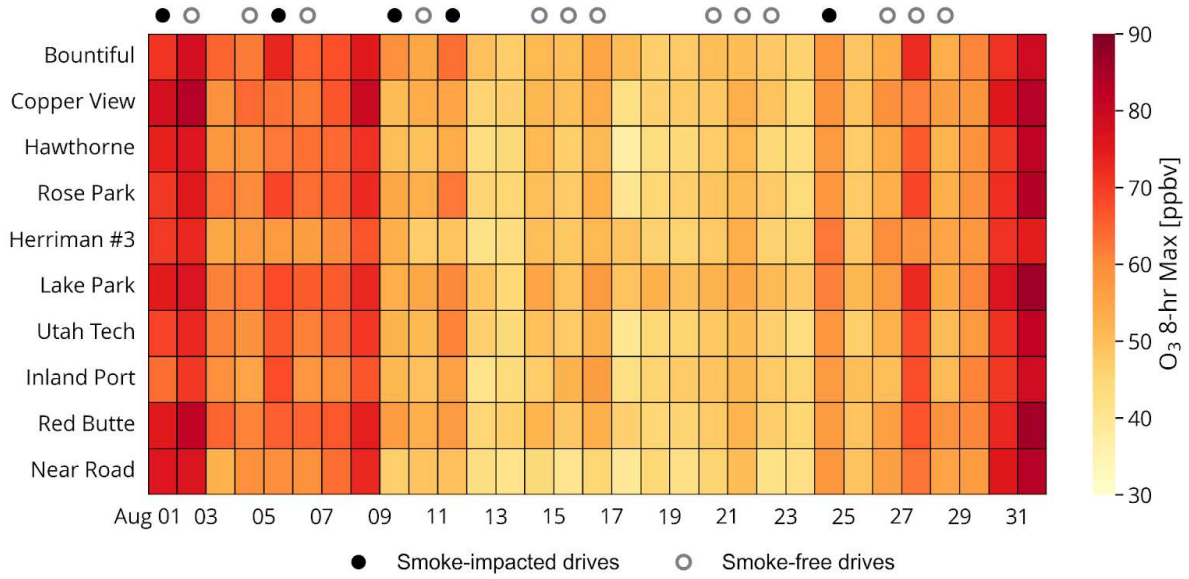

Figure 7. Daily maximum 8-hour average O_3 mixing ratios (ppbv) across monitoring stations in Salt Lake City during August 2024. Each row represents a monitoring site, and each column corresponds to a day. Colored circles in the top indicate the smoke influence status of the drives: smoke-free (white) and smoke-impacted (gray). Plot credit: Brandon McGuire.

3.2 NO_x Distributions in Salt Lake City

3.2.1 Ambient NO_x Abundances and Comparison to Nearby Urban Areas

Using the SIBaR method, we calculated and compared (Table 3) the average on-road background concentrations of NO_x, CO_2, and CO from smoke-free drives conducted in Salt Lake

City, UT during August 2024 with mobile measurements previously reported for Las Vegas, NV and Los Angeles, CA for the period June - September 2021 (Zuraski et al., 2025). In this analysis, the hyper-local plumes have been filtered, and the background represents ambient concentrations for each drive that aim to include broader urban and anthropogenic influences. In August 2024, we observed higher mean NO_x (7.7 ± 4.4 ppbv) and CO (185.9 ± 39.1 ppbv) background levels in Salt Lake City than previous observations for Las Vegas. While we completed our calculations of background values for Salt Lake City using only smoke-free drives, the datasets from Las Vegas and Los Angeles do not specify if smoke-impacted days were excluded, which may explain the higher values of CO observed in LA. Reports from August - September, 2021 show that smoke from Northern California wildfires reached the LA region, potentially influencing the ambient CO concentrations observed in that dataset (Smith, 2021).

Location	Dates	NO_x, ppbv	CO_2, ppmv	CO, ppbv
Salt Lake City, UT	August, 2024	7.7 (4.4)	451.5 (16.7)	185.9 (39.1)
Las Vegas, NV	June, July, and Sep., 2021	5.4 (2.8)	424 (7)	150 (40)
Los Angeles, CA	August and Sep., 2021	12.5 (8.1)	440 (12)	300 (90)

Table 3. Average background concentrations for various cities for smoke-free days. Average deviation is given in parentheses.

3.2.2 NO_2/NO_x Ratios

We applied a plume-by-plume method to isolate direct vehicle exhaust plumes from mobile measurements; then for each plume, the NO_2/NO_x ratio was calculated using the total oxidant approach. For the 19 smoke-free drives, this method captured a total of 878 NO_x plumes. Figure 8a shows the distribution of all valid NO_2/NO_x ratios, with most values falling between 0.05 and 0.15. The arithmetic mean of the ratios was 0.1186 ± 0.1030, while both the geometric mean (0.0821 ± 0.9885) and median (0.0941) were lower, highlighting the asymmetry in the

distribution. This pattern is displayed in Figure 8b, where the log-transformed ratios follow a Gaussian curve, suggesting a log-normal distribution consistent with prior on-road emissions studies (Wild et al., 2017; Zuraski et al., 2025). When dividing by weekday and weekend periods (Table 4), the arithmetic mean NO_2/NO_x ratios is 0.1206 ± 0.1042 on weekdays and 0.0909 ± 0.0804 on weekends, indicating slightly NO_2 fractions on weekends. This pattern is consistent with other U.S. urban observations showing reduced heavy-duty diesel activity and NO_x emissions on weekends (Marr & Harley, 2002; Simon et al., 2024), reflecting a shift toward a larger contribution from gasoline vehicles, which typically emit lower NO_2/NO_x ratios.

The histogram peak for all drives at 0.0647 suggests that most plumes are fresh exhaust emissions, likely from gasoline vehicles which typically emit lower NO_2 fractions and result in lower NO_2/NO_x ratios compared to diesel vehicles (Wild et al., 2017). This likely indicates a predominance of gasoline engines in the fleet, at least in the regions where we sampled. However, despite this distribution, the average NO_2/NO_x ratio is relatively high, suggesting that additional factors may also contribute to the overall elevated ratios, such as fleet composition (Xiang et al., 2022) and emissions control technologies (Carslaw et al., 2016). Emissions inventory data (Figure 2) show that diesel engines represent the largest source of NO_x emissions in Salt Lake and Davis counties, with on-road diesel heavy-duty vehicles contributing about 34% of mobile NO_x emissions compared to 27% from non-diesel light-duty vehicles (Figure 2). There is also a small possibility that this method of plume identification includes other local sources of NO_x, including power generation as there are several in the SLC region. Our measurements were conducted in the summer, and afternoon temperatures >37°C (Figure A11); however, additional analyses presented in the Appendix V, Section B confirm that air temperature was not correlated with the NO_2/NO_x ratios (Figure A12) and the van's driving speed had no significant effect on the results (Figure

A13). Further tests using stricter criteria showed that plumes with more than five valid observations (N = 876) had a mean ratio of 0.115 ± 0.100 (Figure A14, Table A2), while those with $R^2 > 0.6$ (N = 285) had a mean of 0.172 ± 0.123 (Figure A15, Table A3), indicating that stronger linear fits correspond to higher NO_2 fractions.

The average NO_2/NO_x ratio measured in Salt Lake City (11.9 ± 10.3 vol%) is significantly higher than those previously reported for other U.S. cities using the same plume identification algorithm and O_x fitting method, including Las Vegas, NV in 2021 (5.9 ± 0.4), Los Angeles, CA in 2021 (6.3 ± 0.5), and Denver/Greeley, CO in 2014 (5.3), as shown in Table 5. One methodological difference among these studies is that these cities use a different threshold to identify the plumes. Denver and Las Vegas applied 30 ppbv/s threshold and Los Angeles 25 ppbv/s. In this study, we used a 20 ppbv/s threshold, but also tested the other two for comparison, finding that while the number of plumes changed with each threshold, the NO_2/NO_x ratios in Salt Lake City remained consistently high (see Appendix V, Section F). There is a notable exception in an earlier Las Vegas study from 2008-2010, which reported much higher values (25-35%). However, a different methodology was used, based on hourly data from a near-road monitoring network near the I-15 and a statistical model that captured air mixed with the urban background and influenced by rapid chemical conversion of NO to NO_2 (Richmond-Bryant et al., 2017). The I-15 corridor through Las Vegas is a major commuter route with substantial heavy-duty truck activity, which likely enhanced local NO_x concentrations and contributed to the higher NO_2/NO_x ratio reported in this study.

On a global scale, Salt Lake City values are lower than those reported in some urbanized or industrialized Asian and European cities, such as Chengdu, China in 2020 (32.9-50.1%) and Haerkingen, Switzerland in 2004 (23%), but comparable to other locations, including Seoul, Hong

Kong, and Rotterdam. It is important to note that many of these international studies (none of them include tunnel measurements) report ambient or roadside average ratios rather than plume measurements, which may explain the observed differences. The increase of NO_2/NO_x in European cities has been largely linked to a higher share of diesel vehicles and associated control technology (Linn, 2014). These plume-based measurements provide valuable constraints for improving vehicular emissions inventories, particularly in the U.S. cities which appear to largely be shifting to NO_x-limited O_3 chemistry (Koplitz et al., 2021).

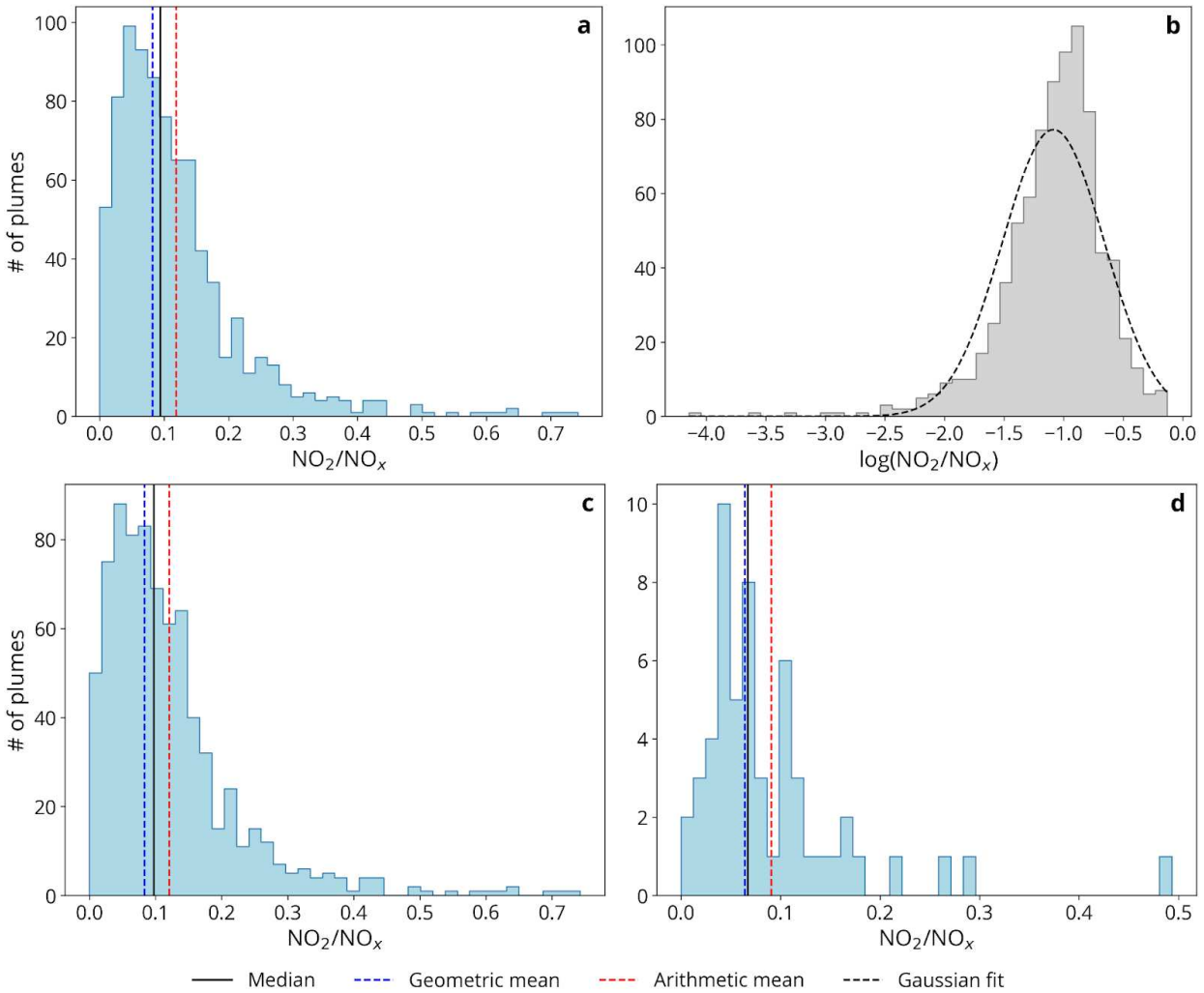

Figure 8. Histogram distribution of NO_2/NO_x ratios for smoke-free drives using a 20 ppbv/s threshold. (a) Full distribution of valid plumes, with vertical lines indicating the median (black, solid line), geometric mean (blue, dashed line), and arithmetic mean (red, dashed line); (b)

distribution of the logarithm of NO_2/NO_x with a fitted Gaussian curve (black, dashed line); (c) weekday plume distribution; and (d) weekend plume distribution.

	All drives	Weekdays	Weekends
Total # of plumes	878	821	57
Arithmetic mean	0.119 ± 0.103	0.121 ± 0.104	0.091 ± 0.080
Geometric mean	0.082 ± 0.989	0.084 ± 0.982	0.064 ± 1.046
Median	0.094	0.097	0.067
Histogram peak	0.065	0.068	0.061

Table 4. Statistical values of NO_2/NO_x ratios from smoke-free drives for all drives (n = 18), weekdays (n = 15) and weekends (n = 3) for a threshold of 20 ppbv/s.

Location	Year(s)	NO_2/NO_x vol%	Reference
Salt Lake City, UT	2024	11.9 (10.3)	This work
Las Vegas, NV	2021	5.9 (0.4)	(Zuraski et al., 2025)
Los Angeles, CA	2021	6.3 (0.5)	(Zuraski et al., 2025)
Chengdu, China	2020	32.9-50.1	(Xiang et al., 2022)
Hong Kong, China	2020	8	(Brimblecombe et al., 2023)
Denver/Greeley, CO	2014	5.3	(Wild et al., 2017)
Las Vegas, NV	2008-2010	25-35	(Richmond-Bryant et al., 2017)
Helsinki, Finland	2009	20	(Anttila et al., 2011)
Seoul, South Korea	1996-2009	11-19	(Shon et al., 2011)
Hong Kong, China	2008	13	(Tian et al., 2011)
Tokyo, Japan	2008	7.3	(Minoura & Ito, 2010)
Rotterdam, Netherlands	2006	13	(Tian et al., 2011)
Haerkingen, Switzerland	2004	23	(Hueglin et al., 2006)
Multiple sites in Europe	2004	12.4	(Grice et al., 2009)
London, UK	2003	17	(Carslaw, 2005)

Multiple sites in Europe	2000	8.6	(Grice et al., 2009)
Helsinki, Finland	1990s	< 10	(Anttila et al., 2011)
Hong Kong, China	1998	2	(Tian et al., 2011)
London, UK	1997	5-6	(Carslaw, 2005)
Rotterdam, Netherlands	1986	9	(Tian et al., 2011)
Haerkingen, Switzerland	1992	14	(Hueglin et al., 2006)

Table 5. NO_2/NO_x ratios (volume %) comparison for various cities from 1986-2024. Average deviation is given in parentheses.

3.2.3 Regional NO_x gradients

There are large gradients in the abundance of NO_x in the Salt Lake City area, with potential implications for O_3 formation in the region. Figure 9 presents regional NO_x maps that show the average NO_x concentrations from the 19 smoke-free drives together with the 10 DAQ monitoring sites located near the mobile measurements. The study area was divided into an approximately equal area grid, and we present the mean NO_x concentrations for each grid cell when at least 10 observations are available. Blue boxes highlight the five lowest-NO_x cells, and the orange boxes indicate the five highest-NO_x cells. Three regional maps are shown in Figure 9, the first includes unfiltered data, the second removes short-lived peaks using the plume isolation method, and the third filters hyper-local plumes using the SIBaR method.

The three regional maps (Figure 9 a-c) demonstrate how the plume filtering approach changes the absolute magnitude of NO_x; however, each approach reveals an east-west spatial gradient. In the SLC region, we generally observed the lowest daytime NO_x abundances toward the west and the highest concentrations toward the east between Bountiful and Copper View. The unfiltered data show the strongest gradient, with differences between low (blue) and high (orange) NO_x areas from an average of ~30 to 50 ppbv. After applying the plume isolation method, the non-plume averages drop, but a gradient of > 25 ppbv is still present. The SIBaR method further reduces

the contrast between these areas to 4 - 5 ppbv. This reflects its more conservative plume-reduction filter and the important contribution of vehicle traffic to NO_x abundances in this region. The absolute concentrations derived from the SIBaR method agree more closely with stationary regulatory observations, supporting the average ambient NO_x abundances value stated in Table 3.

Despite the differences in absolute average NO_x values, all three approaches identify elevated daytime NO_x close to the Near Road, Rose Park, Utah Tech, and Copper View monitoring sites. These patterns align with the stationary diurnal profiles, where the highest daily average NO_x mixing ratios range from ~8-16 ppbv at Near Road, Utah Tech, Rose Park, and Cooper View (Figure 10), compared to < 3 ppbv at Herriman and Red Butte. Both mobile and stationary observations confirm that the Near Road station, located next to major interstate highways, has the highest and most variable NO_x, while western locations, such as Inland Port experience lower (~5.9 ppbv) and less variable NO_x mixing ratios. We consistently sampled the highest NO_x amounts in the region between Bountiful and Rose Park, but there is not a monitoring site there. Adding stationary observations in this area would be valuable for assessing exposure (Collins et al., 2022; Collins & Grineski, 2019).

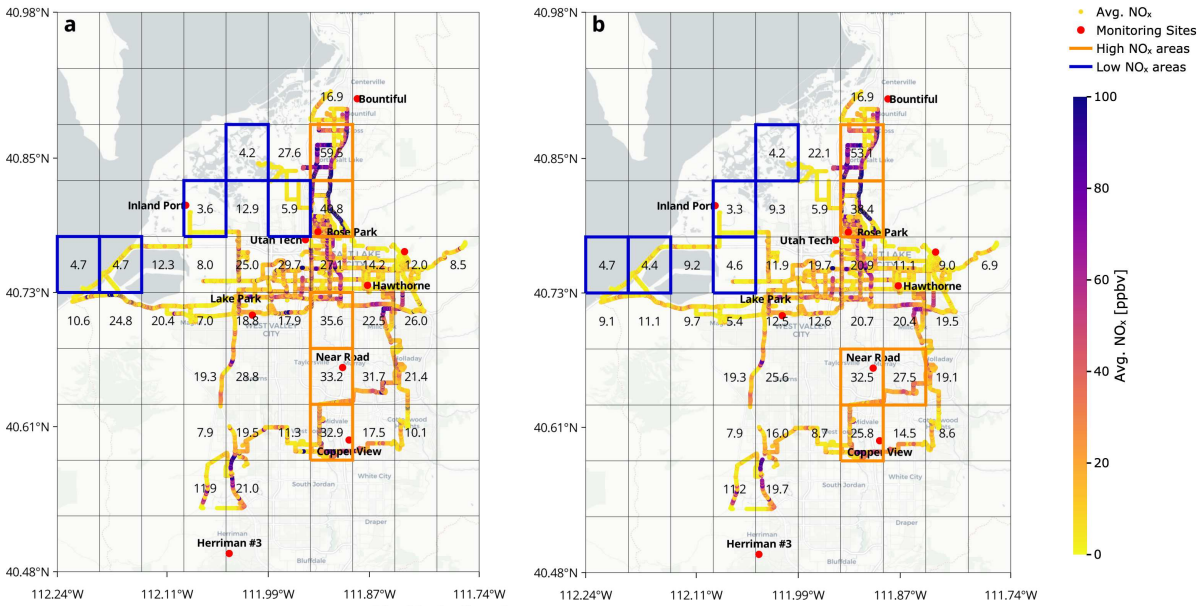

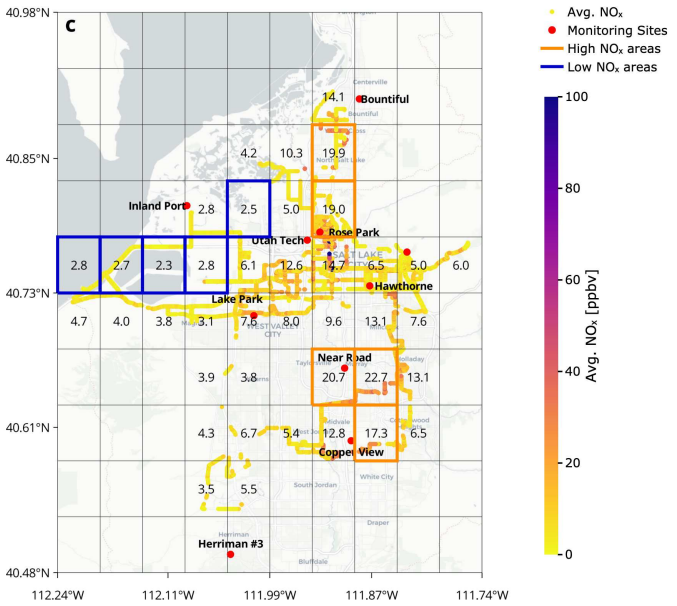

Figure 9. NO_x Regional Maps for smoke-free drives across the Salt Lake Valley in August 2024: (a) unfiltered data, (b) plume isolation method, and (c) SIBaR method. Grid cells (5.6 x 4.2 km) show average NO_x [ppbv]. Orange boxes mark the five highest-NO_x areas and blue boxes the five lowest NO_x areas. DAQ Monitoring Sites are shown as red dots. The 10 x 10 regional grid boxes are 5.6 km N-S x 4.2 km E-W.

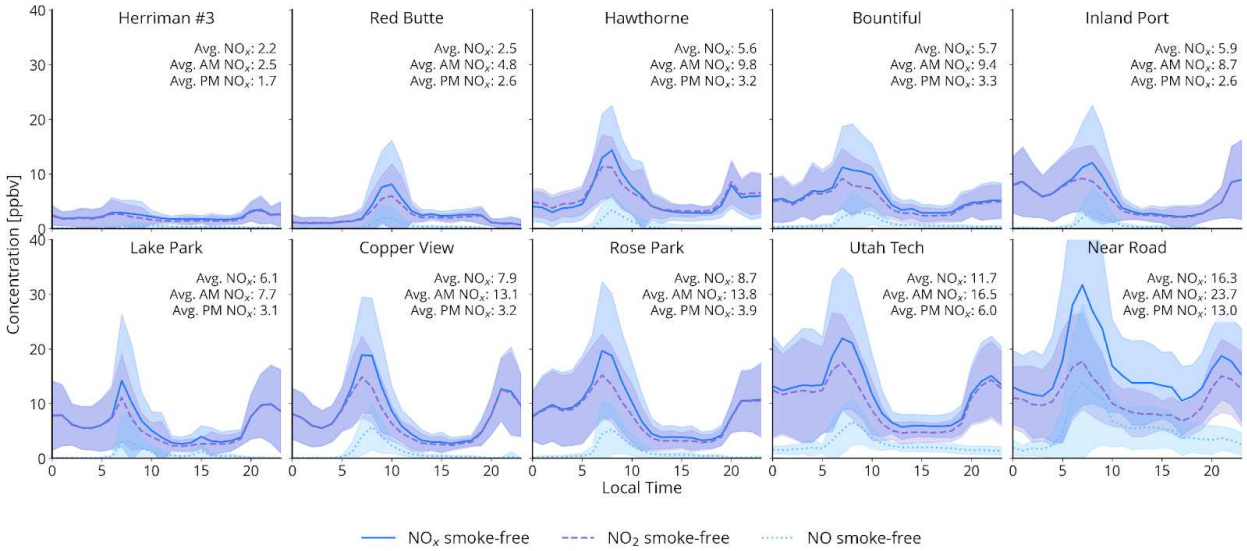

Figure 10. Average diurnal profiles in MDT of NO_x (solid blue), NO_2 (purple dashed), and NO (sky-blue dotted) on smoke-free days at ten DAQ Monitoring Sites during August 2024. Panels are ordered from the lowest to the highest NO_x. The lines indicate the mean in 1 hour and the shaded regions around are 1 standard deviation from the mean. In each panel, the three reported values correspond to the August 2024 monthly average NO_x [ppbv], the average AM NO_x [ppbv] (06:00 AM - 11:59 AM MST), and the average PM NO_x [ppbv] (12:00 PM - 17:59 PM MST).

NO_x levels in SLC vary diurnally, reflecting diurnal characteristics of emissions and chemistry. For the 19 smoke-free drives, we classified 13 as morning drives and 6 as afternoon, including both weekday and weekend observations. First, we focus on the weekday dataset, which includes 5 morning drives (~6:10 AM - 12:50 PM) (excluding the 5 early morning drives before 6:00 AM and Drive 2) and 5 afternoon drives (~11:45 AM - 17:15 PM). For both periods, we can see clear differences in both the magnitude and spatial gradient of NO_x. Figure 11 shows the regional NO_x gradients for weekday-morning drives using both the plume isolation method and SIBaR method. In the morning, there is a strong east-west gradient, with low values in the western part of the valley and the highest values in the east part. There are two factors that may explain the stronger morning gradients: (i) higher emissions from traffic during rush hour, which is also evident in the diurnal NO_x profiles (Figure 10), where concentrations peak between 7 - 9 AM, and (ii) a shallow boundary layer with limited vertical mixing and lower horizontal winds speeds in the morning, favoring pollutant accumulation near the surface (Horel et al., 2016). The DAQ stationary diurnal profiles confirm this pattern, with the highest morning averages (Avg. AM NO_x) at Near Road, Utah Tech, Rose Park, and Cooper View, compared to much lower values at Herriman and Red Butte. Near Road site, which has the highest morning NO_x, exceeds the Herriman site, the cleanest location, by a factor of 10 when comparing average concentrations. In addition, the highest absolute NO_x values in the morning regional maps are again consistently found between Bountiful and Rose Park, where no monitoring site is present, highlighting this gap in the stationary network.

There is a different regional gradient in NO_x abundances in the SLC area in the afternoon than in the morning; during the afternoon, higher NO_x abundances are located further south. For the plume isolation method, the difference between low (blue) and high (orange) NO_x areas is ~11

- 50 ppbv, while the SIBaR method produces a much smaller gradient on the order of a few ppbv. This different spatial pattern likely reflects both meteorological and chemical processes. All weekday-afternoon smoke-free drives followed the Lake Breeze Front Route (Figure 3); three drives occurred under northwesterly winds (Figure A18) and two were conducted during southerly or variable wind conditions. Figure A18 illustrates the wind shift associated with the Lake Breeze Front Route, with morning southerly flow transitioning to northwesterly winds in the afternoon. Under these conditions, it appears that emissions from the Bountiful area may have been transported south. The distribution in Figure 11 is consistent with observations at the stationary sites (Figure 10); the highest afternoon concentrations (Avg. PM NO_x) occur at Near Road (Figure A19). We did not conduct weekday afternoon drives near the Near Road site, which still shows the highest NO_x concentrations; this should be considered in future work.

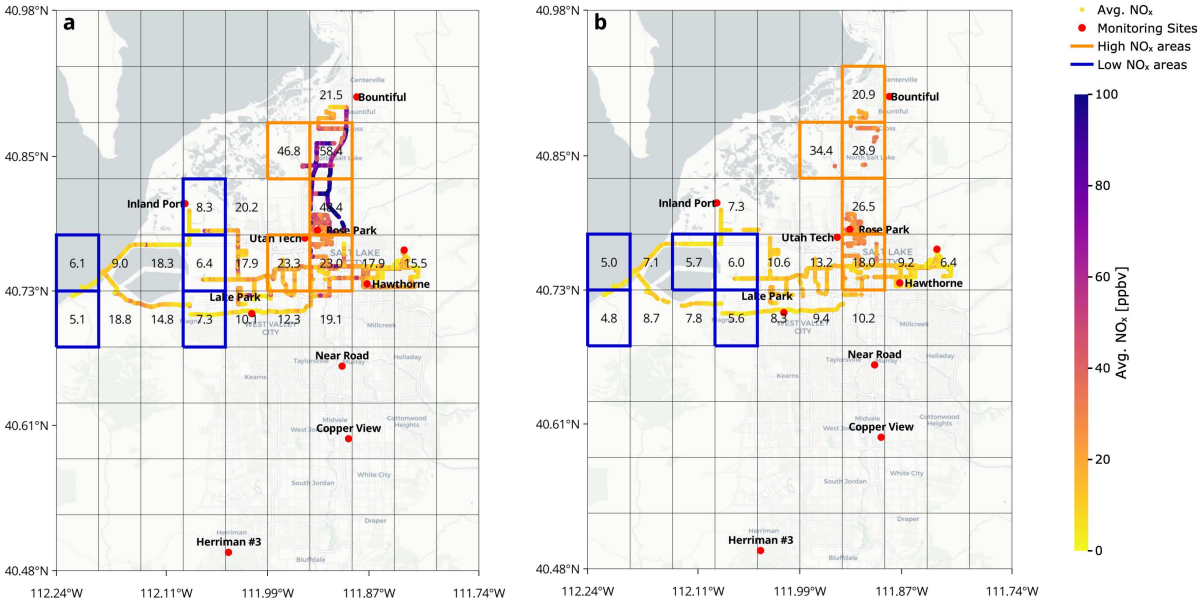

Figure 11. NO_x Regional Map for smoke-free weekday morning drives (~6:10 AM - 12:50 PM MST) across the Salt Lake Valley in August 2024: (a) plume isolation method and (b) SIBaR method. Grid cells (5.6 x 4.2 km) show average NO_x [ppbv]. Orange boxes mark the five highest-NO_x areas and blue boxes the five lowest NO_x areas. DAQ Monitoring Sites are shown as red dots.

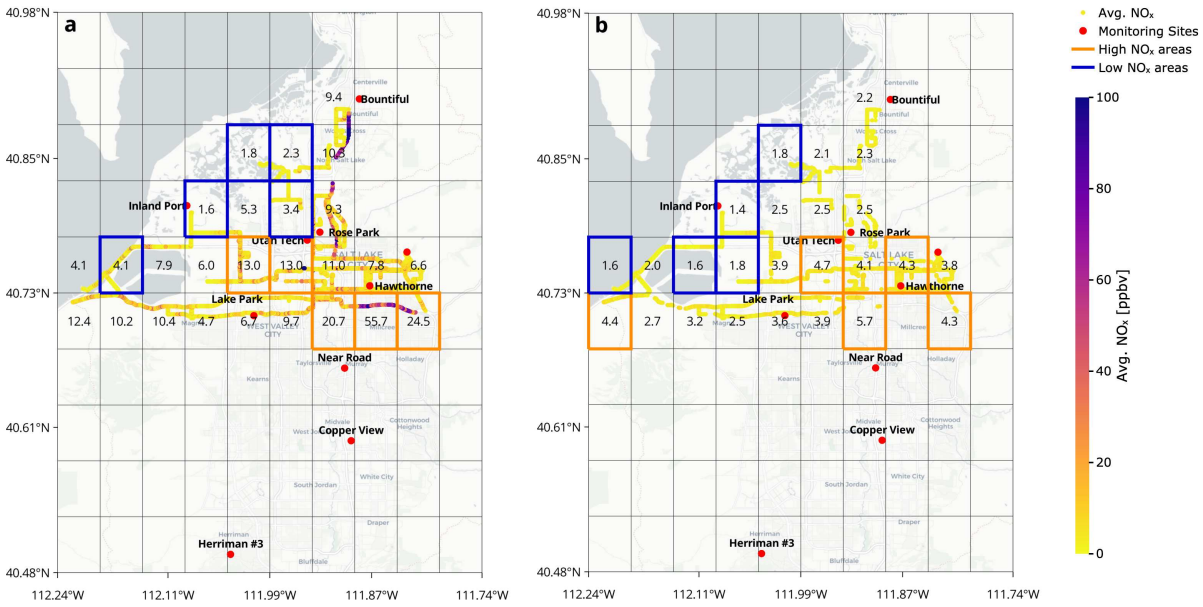

Figure 12. NO_x Regional Map for smoke-free weekday afternoon drives (~11:45 AM - 17:15 PM MST) across the Salt Lake Valley in August 2024: (a) plume isolation method and (b) SIBaR method. Grid cells (5.6 x 4.2 km) show average NO_x [ppbv]. Orange boxes mark the five highest-NO_x areas and blue boxes the five lowest NO_x areas. DAQ Monitoring Sites are shown as red dots.

3.2.4 Weekday-Weekend Differences

Differences in NO_x abundances between weekdays and weekends, driven by changes in anthropogenic activities, can reveal the contribution of traffic to regional NO_x and its effect on O_3 production (Abeleira & Farmer, 2017; Cleveland et al., 1974; Pollack et al., 2012; Pusede & Cohen, 2012). To investigate these differences, we analyzed regional maps and the distribution of observations from the subset of filtered observations using both the plume isolation method and the SIBaR methods; we also conducted a comparison using the routine observations from the DAQ monitoring sites. Figures 11 and 12 present the NO_x regional maps for smoke-free days during both morning and afternoon periods: (a) 10 weekday drives (~06:10 AM - 17:15 PM MST), excluding early morning drives and Drive 2; (b) 3 weekend drives (~09:00 AM - 16:45 PM MST), and (c) the average weekdays-weekends differences where data from both are available and positive. Figure 15 presents boxplots comparing the lowest (blue) and highest (orange) NO_x areas identified in the regional maps, and Figure 16 shows boxplots for the 10 DAQ monitoring sites on

smoke-free Wednesdays (W = 3) and Sundays (S = 2) using a similar approach to that described in Pollack et al., (2021). These days were chosen because they represent typical weekday and weekend conditions, unaffected by emissions from transitional days (Heuss et al., 2003; Murphy et al., 2007). Wednesdays were selected to represent a typical midweek day, and Sundays were chosen because they represent a significant minimum in NO_x emissions as a traditional rest day in North American cities (Stavrakou et al., 2020). No holidays affecting local emissions were identified during the field campaign. Due to the limited number of smoke-free Wednesdays and Sundays in August, additional boxplots are included in the Appendix VII, to account for the variability with longer periods. These include (i) August including both smoke-free and smoke impacted Wednesdays and Sundays (Figure A20); (ii) all summer months from June to September 2024, including both smoke-free and smoke-impacted Wednesdays and Sundays (Figure A21); and (iii) all summer months from June to September including both smoke-free and smoke-impacted Wednesdays and Saturdays (Figure A22).

Both filtering approaches (Figure 13a-c and 14a-c) reveal an east-west spatial gradient during both weekdays and weekends, with maximum NO_x abundances between the Bountiful and Utah Technological Center sites, which are both located near major roadways and strongly influenced by vehicular emissions. Minimum concentrations are present over the western area of the valley. On weekends, this gradient persists but with substantially lower magnitudes. For the plume isolation method, weekday magnitudes drop from an average of ~43 to 49 ppbv to only ~3 to 4 ppbv on weekends (Figure 13c). The lowest-NO_x areas experience ~52% reduction and the highest-NO_x areas an even larger ~66% reduction between weekdays and Sundays (Figure 15). The SIBaR method produced similar results but with even bigger differences. This approach indicates that there is a ~58% reduction in the western low-NO_x areas and a ~80% reduction in the

eastern high-NO_x areas on Sundays versus weekdays. These results demonstrate that while the east-west spatial gradient persists, weekend NO_x abundances are substantially lower (by about 50-80%) compared to weekdays, reflecting the sharp decline in roadway traffic and commuters on the weekends, a pattern that has been reported in large urban areas, including Salt Lake City (Kuprov et al., 2014; Valin et al., 2014).

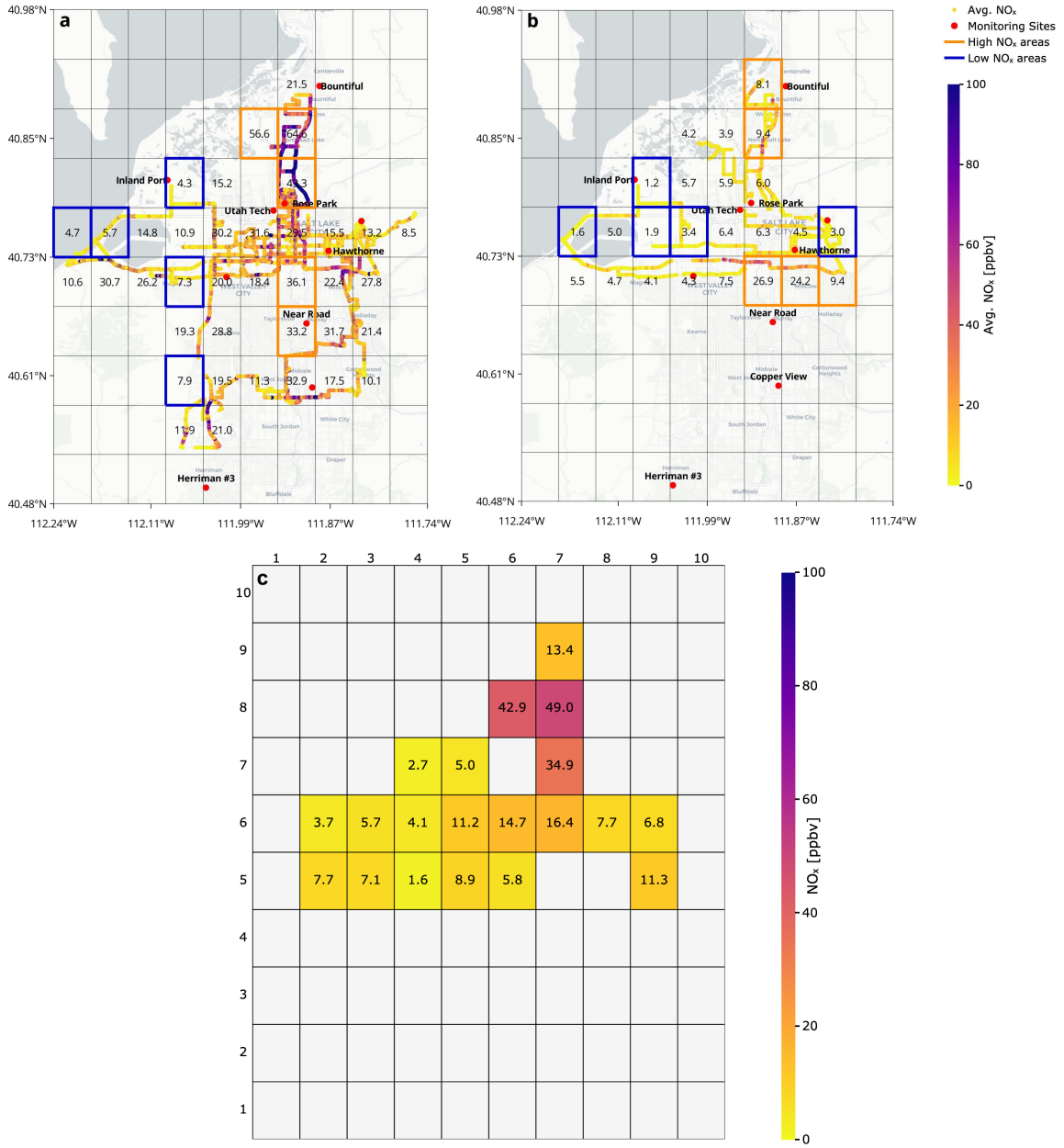

Figure 13. NO_x Regional Maps for smoke-free drives across the Salt Lake Valley in August 2024 using the plume isolation method: (a) weekdays (~06:10 AM - 17:15 PM MST), (b) weekends (~09:00 AM - 16:45 PM MST), and (c) average weekday-weekend differences. Grid cells (5.6 x 4.2 km) show average NO_x [ppbv]. Orange boxes mark the five highest-NO_x areas and blue boxes the five lowest NO_x areas. DAQ Monitoring Sites are shown as red dots.

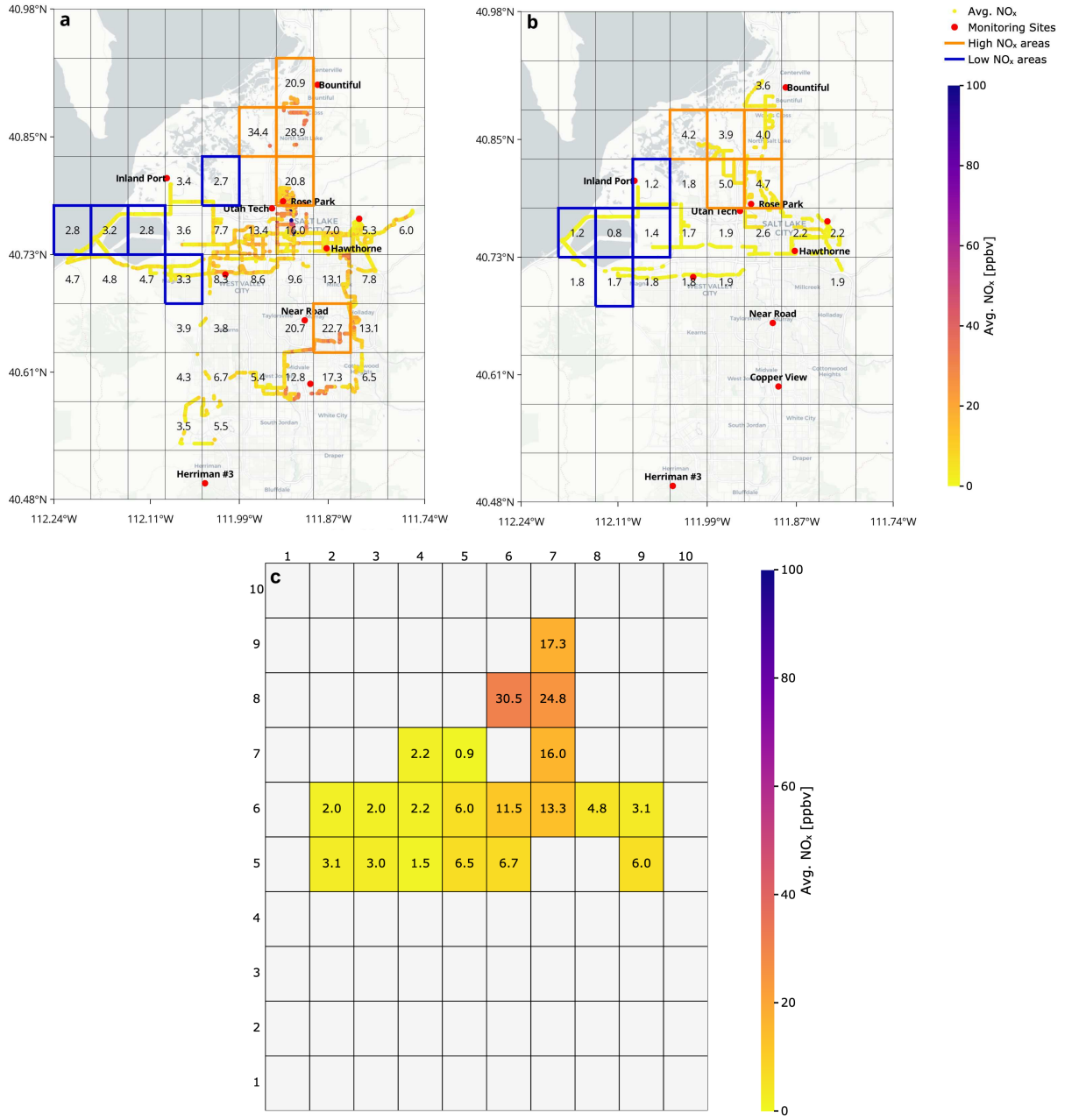

Figure 14. NO_x Regional Maps for smoke-free drives across the Salt Lake Valley in August 2024 using the SIBaR method: (a) weekdays (~06:10 AM - 17:15 PM MST), (b) weekends (~09:00 AM - 16:45 PM MST), and (c) average weekday-weekend differences. Grid cells (5.6 x 4.2 km) show average NO_x [ppbv]. Orange boxes mark the five highest-NO_x areas and blue boxes the five lowest NO_x areas. DAQ Monitoring Sites are shown as red dots.

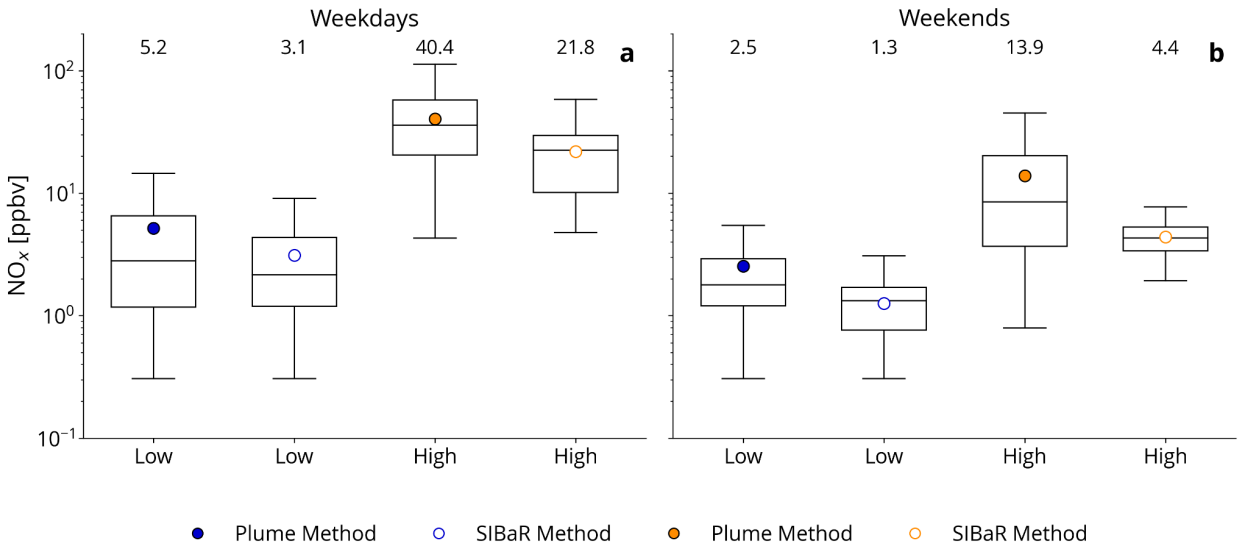

Figure 15. Boxplots of NO_x mixing ratios for low and high areas from the regional smoke-free maps for (a) weekdays and (b) weekends. Note the y-axis is a logarithmic scale. Boxes extend from the 25th to 75th percentile, whiskers extend from the minimum to the maximum values, and the median is indicated by the horizontal line across each box. Colored circles represent the mean values for the plume isolation method (solid blue and orange) and SIBaR method (open blue and orange) and numeric values above each box plot indicate the mean NO_x concentration.

Stationary observations at the DAQ monitoring sites provide additional evidence of weekday-weekend differences in NO_x and corroborate the spatial pattern identified in the regional maps. Figure 16 shows substantially lower NO_x values on Sundays (S) compared to Wednesdays (W), with reductions > 70% at high-NO_x locations, such as Utah Tech, Rose Park, and Copper View. Other eastern sites, including Bountiful and Hawthorne, also showed significant decreases of ~67%. Western sites such as Inland Port exhibit smaller reductions (~20%), while Lake Park shows a moderate decrease of ~59%. When comparing Wednesdays with Saturdays (Figure A21) for all summer (June to September), reductions are still evident, and Sundays consistently show the lowest NO_x values. These observations are consistent with the findings of SAMOZA, where the lowest NO_x values were found on Saturday and Sunday (Jaffe et al., 2024), highlighting the dominant influence of traffic emissions in regional NO_x distributions and the cultural context of

Salt Lake City, where commuting is especially reduced on Sundays due to the predominant Mormon community.

The lowest mean NO_x concentration was measured at Herriman #3. During the limited days available for comparison in August 2024, the data collected at this site shows an increase in NO_x (~33%) on Sundays compared to Wednesdays. Meteorological conditions in August were comparable between Sundays (S) and Wednesdays (W) with daily maximum temperatures differing by only a few degrees across sites (Figure A23), and similar wind flow patterns (south - southeasterly) for the smoke-free days at the monitoring sites (Figure A19). This likely reflects the limited number of smoke-free Sundays considered in Figure 16. If we consider all days in August or all summer months (June to September), including both smoke-free and smoke-impacted days (Figure A20 and Figure A21), there is a decrease in NO_x abundances at Herriman #3 of ~29% or 59% respectively, consistent with the other monitoring sites. This shows the sensitivity to the averaging period for this calculation, particularly at locations without strong week-day vehicle emissions. The Herriman #3 site is located in the far southwestern corner of the valley and is not as strongly influenced by urban traffic or commuter activity as other locations; therefore, its weekday-weekend difference is weaker. This is also an example of how NO_x distributions vary across the region, and how this likely produces different O_3 chemistry. When all summer days are considered, only Inland Port (~51%) and Near Road (~65%) show stronger reduction, while the other stations keep similar differences to those observed in August. Therefore, the smoke-free sample size is not sufficient to fully capture the weekday-weekend differences during August at some sites. Overall, weekends are cleaner days compared to weekdays, with reductions ranging from ~30% to 75%.

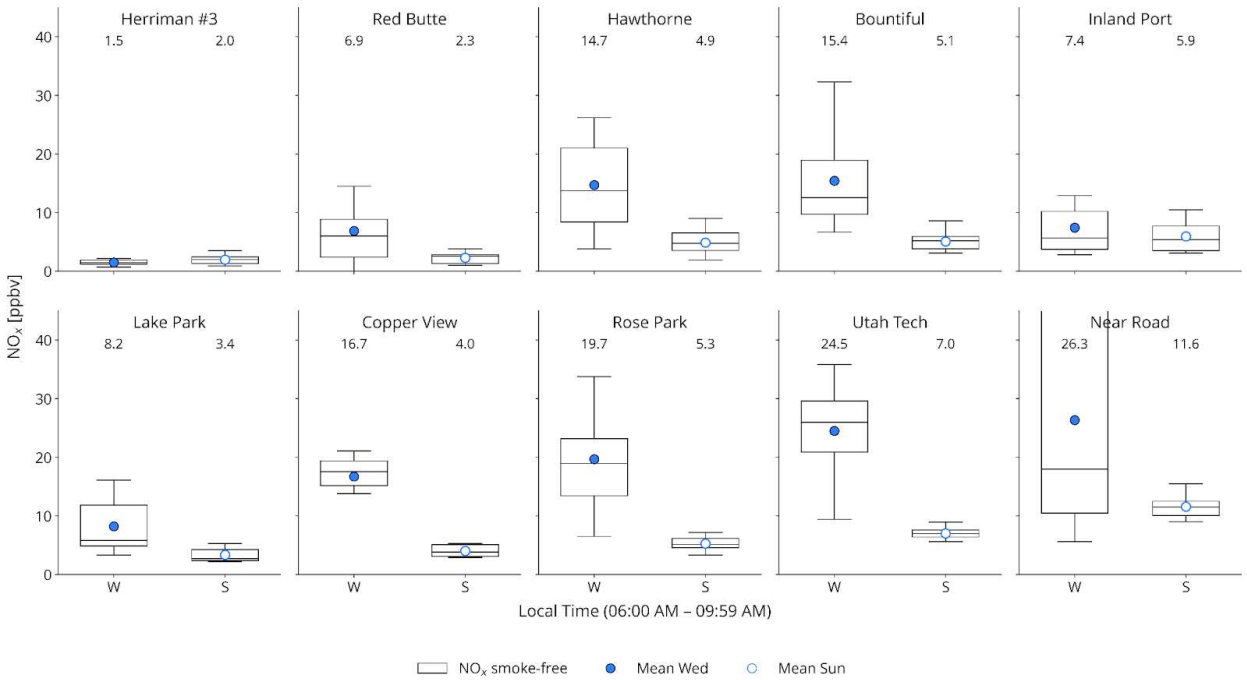

Figure 16. Boxplots of NO_x mixing ratios observed during the morning period (~06:00 AM - 09:59 AM) for the ten DAQ monitoring sites during August 2024 for smoke-free days. Panels follow the same site order as the diurnal profiles. Boxes extend from the 25th to 75th percentile, whiskers extend from the minimum to the maximum values, and the median is indicated by the horizontal line across each box. Colored circles represent the mean values for Wednesday (solid blue) and Sunday (open blue) and numeric values above each box plot indicate the mean NO_x concentration.

CHAPTER 4 : CONCLUSIONS AND FUTURE WORK

Salt Lake City experiences frequent exceedances of the NAAQS for O_3 in the summer. As part of the 2024 SLC-SOS field campaign, we deployed the CAPS monitor in a mobile laboratory to quantify regional gradients and daily variability of NO_x across the Salt Lake Valley. Our analysis includes: (1) ambient NO_x abundances using the SIBaR method and NO_2/NO_x ratios from vehicle exhaust plumes using the total oxidant approach with a comparison to nearby urban areas; (2) regional maps of NO_x gradients and morning-afternoon differences; and (3) weekday–weekend differences in NO_x distributions across regulatory monitoring sites and mobile transects on smoke-free days.

Key results from our analysis include:

- Ambient NO_x abundances in Salt Lake City determined using mobile measurements are higher than those previously reported for Las Vegas and comparable to Los Angeles, with near source filtered levels of 7.7 ± 4.4 pppb for NO_x, 185.9 ± 39.1 ppbv for CO, and 451.5 ± 16.7 ppmv for CO_2. While our dataset only includes smoke-free drives, the data from the other cities may include smoke-impacted days, potentially contributing to the elevated CO observed in Los Angeles in 2021.
- The average NO_2/NO_x ratio in individual plumes is 11.9 ± 10.3%, about twice as high as other U.S. cities, but comparable to other international cities, likely reflecting differences in fleet composition, with Salt Lake and Davis counties having a higher proportion of diesel heavy-duty vehicles
- We estimated regional gradients using multiple methods and found that there are large east-west gradients in NO_x across Salt Lake City. Unfiltered data showed the strongest gradient (~30 to 50 ppbv), the plume isolation method revealed > 25 ppbv gradient, and the SIBaR

method reduced the difference to ~4 – 5 ppbv. The highest abundances are between Bountiful and Copper View sites, while the lowest is at Inland Port, consistent with the DAQ monitoring stations that report maximum NO_x averages at Near Road (16.3 ppbv) and Utah Tech (11.7 ppbv) and minima at Herriman #3 and Red Butte (< 3ppbv).

- On weekdays, NO_x shows strong diurnal variability: mornings exhibit a strong east-west gradient, with Near Road exceeding Herriman #3 by a factor of ~10, likely driven by rush hour traffic; while in the afternoon, the highest abundances shift southward, with gradients of ~11 to 50 ppbv using the plume isolation method and only a few ppbv with the SIBaR method, reflecting transport under northwesterly winds.
- Weekday-weekend differences show that NO_x decreases on weekends by ~50 to 80% across Salt Lake City, with the strongest reductions at high-NO_x regions (i.e., near Utah Tech, Rose Park, and Copper View), and smaller decreases at western areas, e.g., Inland Port. This pattern is consistent with the DAQ monitoring sites, which also report >70% reductions at urban locations and weaker signals at peripheral sites like Herriman, with Sundays consistently showing the lowest abundances.

The observations and analysis presented above provide a key steppingstone for several different avenues of future work. They fall into 5 categories: 1) Plume composition ratios and emission inventories, 2) weekday - weekend differences in O_3 versus NO_x, 3) smoke versus no-smoke differences and implications for O_3 formation, 4) extension to airborne measurements (i.e., SLC-SOS 2026), and 5) comparison with similar datasets including USOS 2024 and FROZÉ 2025.

1. Plume composition ratios and emission inventories

For smoke-free days, we can calculate additional plume composition ratios (e.g., NO_x/CO_2, NO_x/CO, and CO/CO_2) and compare them with other U.S. cities to assess regional variability. This

analysis can be extended to estimate on-road vehicle fuel consumption from both light duty gasoline vehicle and heavy-duty diesel vehicles, calculate pollutant emissions by applying fuel-base emissions factors (g pollutant/kg fuel), and update the Fuel-based Inventory for Vehicle Emissions (FIVE) for Salt Lake City following the methodology of Zuraski et al., (2025).

2. Weekday - weekend differences in O_3 versus NO_x

For smoke-free days, the next step is to examine weekday-weekend differences in NO_x emissions together with changes in O_3 and O_3 production efficiency (OPE) using a day of the week (DOW) analysis to assess whether local air quality in Salt Lake City is transitioning toward NO_x-limited O_3 production, as observed in other U.S cities (Koplitz et al., 2021; Simon et al., 2024b) or remains largely NO_x-saturated (Cope et al., 2024). This analysis would help understand the chemical drivers for O_3 formation in the region and guide effective emission control strategies.

3. Smoke versus no-smoke differences and implications for O_3 formation

Given that we have already identified smoke-impacted days during the August 2024 campaign (Figure 4), we could easily follow the methodology of Lindaas et al., (2017) to characterize smoke versus smoke-impacted differences in composition. We hypothesize that during smoke-impacted periods, (1) NO_x abundances do not significantly change relative to smoke-free periods, but (2) there are significant increases in the abundance of VOCs (Permar et al., 2021; Rickly et al., 2023; Xu et al., 2021). Preliminary analysis using stationary data is presented in the Appendix VIII. These plots include: i) diurnal profiles that compare NO_x and O_3 under smoke-free and smoke-impacted conditions (Figure A24), ii) the distribution of O_3 and its dependence on temperature using histograms scatter plots and boxplots (Figure A25), and iii) a time-series of daily maximum O_3 and temperature designating where high O_3 aligned with the presence of wildfire smoke (Figure A26). These analyses can be merged with the smoke-impacted

mobile measurements of NO_x and VOCs to provide a more specific characterization of smoke effects on O_3 and its precursors in this region.

4. Airborne measurements during SLC-SOS 2026

Our team will return to Salt Lake City in the summer of 2026 for the second part of the SLC-SOS field campaign, which will focus on airborne observations. We will have the Wyoming King Air (UWKA) aircraft with the same payload that was deployed on the UW Lab in 2024. Planned flight patterns (i.e., lake-breeze, urban fluxes, and intervalley transport flights) will capture spatiotemporal (vertical and horizontal) gradients in O_3 and its precursors. This second deployment in 2026 will complement the mobile measurements from 2024 by providing information on the vertical evolution of the boundary layer impacting O_3 at the surface.

5. Comparison with USOS 2024 and FROZÉ 2025

There is an opportunity to compare the findings presented here with data collected during both the Utah Summer Ozone Study (USOS 2024) and the Front Range OZone Experiment (FROZÉ 2025). USOS was conducted from 15 July to 18 August 2024, overlapping with SLC-SOS measurements during the first weeks of August. This campaign deployed the NOAA CSL mobile laboratory, the NOAA Twin Otter aircraft, the Air Resources Car (ARC), and remote sensing spectrometers installed at existing UDAQ monitoring sites. FROZÉ was conducted from 26 June to 21 August 2024. This campaign included deployment of the CSU Tahoe with a payload focused on exposure and the University of Montana mobile lab with the same O3-focused payload as the SLC-SOS 2024 mobile lab.

REFERENCES

Abeleira, A. J., & Farmer, D. K. (2017). Summer ozone in the northern Front Range metropolitan area: Weekend–weekday effects, temperature dependences, and the impact of drought. Atmospheric Chemistry and Physics, 17(11), 6517–6529. https://doi.org/10.5194/acp-17-6517-2017

Actkinson, B., Ensor, K., & Griffin, R. J. (2021). SIBaR: A new method for background quantification and removal from mobile air pollution measurements. Atmospheric Measurement Techniques, 14(8), 5809–5821. https://doi.org/10.5194/amt-14-5809-2021

Anttila, P., Tuovinen, J.-P., & Niemi, J. V. (2011). Primary NO2 emissions and their role in the development of NO2 concentrations in a traffic environment. Atmospheric Environment, 45(4), 986–992. https://doi.org/10.1016/j.atmosenv.2010.10.050

Bechle, M. J., Millet, D. B., & Marshall, J. D. (2023). Ambient NO2 Air Pollution and Public Schools in the United States: Relationships with Urbanicity, Race–Ethnicity, and Income. Environmental Science & Technology Letters, 10(10), 844–850. https://doi.org/10.1021/acs.estlett.3c00507

Blaszczak-Boxe, C., Karle, N. N., Ideki, O., Taku, L., Yu, M., Wang, S., Golosov, N., Riyad, M., Hilaire, D. St., Smith, K., Abdul-Hamid, B., Hollet, T., & Quarkume, A. (2025). Temporal variations in NOx, O3, and CO2 and meteorological influences in New York and New Jersey urban atmospheres. Discover Environment, 3(1), 98. https://doi.org/10.1007/s44274-025-00226-6

Blaylock, B. K., Horel, J. D., & Crosman, E. T. (2017). Impact of Lake Breezes on Summer Ozone Concentrations in the Salt Lake Valley. https://doi.org/10.1175/JAMC-D-16-0216.1

Brey, S. J., & Fischer, E. V. (2016a). Smoke in the City: How Often and Where Does Smoke Impact Summertime Ozone in the United States? Environmental Science & Technology, 50(3), 1288–1294. https://doi.org/10.1021/acs.est.5b05218

Brey, S. J., & Fischer, E. V. (2016b). Smoke in the City: How Often and Where Does Smoke Impact Summertime Ozone in the United States? Environmental Science & Technology, 50(3), 1288–1294. https://doi.org/10.1021/acs.est.5b05218

Brimblecombe, P., Chu, M., Liu, C.-H., Fu, Y., Wei, P., & Ning, Z. (2023). Roadside NO2/NOx and primary NO2 from individual vehicles. Atmospheric Environment, 295, 119562. https://doi.org/10.1016/j.atmosenv.2022.119562

Bureau, U. C. (2025). City and Town Population Totals: 2020-2024. Census.Gov. https://www.census.gov/data/tables/time-series/demo/popest/2020s-total-cities-and-towns.html

Carslaw, D. C. (2005). Evidence of an increasing NO2/NOX emissions ratio from road traffic emissions. Atmospheric Environment, 39(26), 4793–4802. https://doi.org/10.1016/j.atmosenv.2005.06.023

Carslaw, D. C., Murrells, T. P., Andersson, J., & Keenan, M. (2016). Have vehicle emissions of primary NO2 peaked? Faraday Discussions, 189(0), 439–454. https://doi.org/10.1039/C5FD00162E

Chang, K.-L., McDonald, B. C., Harkins, C., & Cooper, O. R. (2025). Surface ozone trend variability across the United States and the impact of heat waves (1990–2023). Atmospheric Chemistry and Physics, 25(10), 5101–5132. https://doi.org/10.5194/acp-25-5101-2025

Clark, L. P., Millet, D. B., & Marshall, J. D. (2014). National Patterns in Environmental Injustice and Inequality: Outdoor NO2 Air Pollution in the United States. PLOS ONE, 9(4), e94431. https://doi.org/10.1371/journal.pone.0094431

Cleveland, W. S., Graedel, T. E., Kleiner, B., & Warner, J. L. (1974). Sunday and Workday Variations in Photochemical Air Pollutants in New Jersey and New York. Science, 186(4168), 1037–1038. https://doi.org/10.1126/science.186.4168.1037

Collins, T. W., & Grineski, S. E. (2019). Environmental Injustice and Religion: Outdoor Air Pollution Disparities in Metropolitan Salt Lake City, Utah. Annals of the American Association of Geographers, 109(5), 1597–1617. https://doi.org/10.1080/24694452.2018.1546568

Collins, T. W., Grineski, S. E., & Nadybal, S. M. (2022). A Comparative Approach for Environmental Justice Analysis: Explaining Divergent Societal Distributions of Particulate Matter and Ozone Pollution across U.S. Neighborhoods. Annals of the American Association of Geographers, 112(2), 522–541. https://doi.org/10.1080/24694452.2021.1935690

Commane, R., Hallward-Driemeier, A., & Murray, L. T. (2023). Intercomparison of commercial analyzers for atmospheric ethane and methane observations. Atmospheric Measurement Techniques, 16(5), 1431–1441. https://doi.org/10.5194/amt-16-1431-2023

Cooper, O. R., Langford, A. O., Parrish, D. D., & Fahey, D. W. (2015). Challenges of a lowered U.S. ozone standard. Science. https://doi.org/10.1126/science.aaa5748

Cope, E. M., Ketcherside, D. T., Jin, L., Tan, L., Mansfield, M., Jones, C., Lyman, S., Jaffe, D., & Hu, L. (2024). Sources of Atmospheric Volatile Organic Compounds During the Salt Lake

Regional Smoke, Ozone and Aerosol Study (SAMOZA) 2022. Journal of Geophysical Research: Atmospheres, 129(17), e2024JD041640. https://doi.org/10.1029/2024JD041640

Crosson, E. R. (2008). A cavity ring-down analyzer for measuring atmospheric levels of methane, carbon dioxide, and water vapor. Applied Physics B, 92(3), 403–408. https://doi.org/10.1007/s00340-008-3135-y

Dix, B., de Bruin, J., Roosenbrand, E., Vlemmix, T., Francoeur, C., Gorchov-Negron, A., McDonald, B., Zhizhin, M., Elvidge, C., Veefkind, P., Levelt, P., & de Gouw, J. (2020). Nitrogen Oxide Emissions from U.S. Oil and Gas Production: Recent Trends and Source Attribution. Geophysical Research Letters, 47(1), e2019GL085866. https://doi.org/10.1029/2019GL085866

Donzelli, G., & Suarez-Varela, M. M. (2024). Tropospheric Ozone: A Critical Review of the Literature on Emissions, Exposure, and Health Effects. Atmosphere, 15(7), 779. https://doi.org/10.3390/atmos15070779

Duncan, B. N., Yoshida, Y., Olson, J. R., Sillman, S., Martin, R. V., Lamsal, L., Hu, Y., Pickering, K. E., Retscher, C., Allen, D. J., & Crawford, J. H. (2010). Application of OMI observations to a space-based indicator of NOx and VOC controls on surface ozone formation. Atmospheric Environment, 44(18), 2213–2223. https://doi.org/10.1016/j.atmosenv.2010.03.010

Emberson, L. (2020). Effects of ozone on agriculture, forests and grasslands. Philosophical Transactions of the Royal Society A: Mathematical, Physical and Engineering Sciences, 378(2183), 20190327. https://doi.org/10.1098/rsta.2019.0327

EPA, U. (2015). Green Book | US EPA. https://www3.epa.gov/airquality/greenbook/anayo_ut.html

Erickson, L. E., Newmark, G. L., Higgins, M. J., & Wang, Z. (2020). Nitrogen oxides and ozone in urban air: A review of 50 plus years of progress. Environmental Progress & Sustainable Energy, 39(6), e13484. https://doi.org/10.1002/ep.13484

Fishman, J., Solomon, S., & Crutzen, P. J. (1979). Observational and theoretical evidence in support of a significant in-situ photochemical source of tropospheric ozone | Tellus A: Dynamic Meteorology and Oceanography. https://doi.org/10.3402/tellusa.v31i5.10458

Goldberg, D. L., Anenberg, S. C., Lu, Z., Streets, D. G., Lamsal, L. N., E McDuffie, E., & Smith, S. J. (2021). Urban NOx emissions around the world declined faster than anticipated between 2005 and 2019. Environmental Research Letters, 16(11), 115004. https://doi.org/10.1088/1748-9326/ac2c34

Grice, S., Stedman, J., Kent, A., Hobson, M., Norris, J., Abbott, J., & Cooke, S. (2009). Recent trends and projections of primary NO2 emissions in Europe. Atmospheric Environment, 43(13), 2154–2167. https://doi.org/10.1016/j.atmosenv.2009.01.019

Hannun, R. A., Swanson, A. K., Bailey, S. A., Hanisco, T. F., Bui, T. P., Bourgeois, I., Peischl, J., & Ryerson, T. B. (2020). A cavity-enhanced ultraviolet absorption instrument for high-precision, fast-time-response ozone measurements. Atmospheric Measurement Techniques, 13(12), 6877–6887. https://doi.org/10.5194/amt-13-6877-2020

Heuss, J. M., Kahlbaum, D. F., & Wolff, G. T. (2003). Weekday/Weekend Ozone Differences: What Can We Learn from Them? Journal of the Air & Waste Management Association, 53(7), 772–788. https://doi.org/10.1080/10473289.2003.10466227

Horel, J., Crosman, E., Jacques, A., Blaylock, B., Arens, S., Long, A., Sohl, J., & Martin, R. (2016). Summer ozone concentrations in the vicinity of the Great Salt Lake. https://doi.org/10.1002/asl.680

Hueglin, C., Buchmann, B., & Weber, R. O. (2006). Long-term observation of real-world road traffic emission factors on a motorway in Switzerland. Atmospheric Environment, 40(20), 3696–3709. https://doi.org/10.1016/j.atmosenv.2006.03.020

Jaffe, D. A., Cooper, O. R., Fiore, A. M., Henderson, B. H., Tonnesen, G. S., Russell, A. G., Henze, D. K., Langford, A. O., Lin, M., & Moore, T. (2018). Scientific assessment of background ozone over the U.S.: Implications for air quality management. Elementa: Science of the Anthropocene, 6, 56. https://doi.org/10.1525/elementa.309

Jaffe, D. A., Ninneman ,Matt, Nguyen ,Linh, Lee ,Haebum, Hu ,Lu, Ketcherside ,Damien, Jin ,Lixu, Cope ,Emily, Lyman ,Seth, Jones ,Colleen, O'Neil ,Trevor, & and Mansfield, M. L. (2024). Key results from the salt lake regional smoke, ozone, and aerosol study (SAMOZA). Journal of the Air & Waste Management Association, 74(3), 163–180. https://doi.org/10.1080/10962247.2024.2301956

Jaffe, D. A., & Wigder, N. L. (2012). Ozone production from wildfires: A critical review. Atmospheric Environment, 51, 1–10. https://doi.org/10.1016/j.atmosenv.2011.11.063

Jhun, I., Coull, B. A., Zanobetti, A., & Koutrakis, P. (2015). The impact of nitrogen oxides concentration decreases on ozone trends in the USA. Air Quality, Atmosphere, & Health, 8(3), 283–292. https://doi.org/10.1007/s11869-014-0279-2

Kaulfus, A. S., Nair, U., Jaffe, D., Christopher, S. A., & Goodrick, S. (2017). Biomass Burning Smoke Climatology of the United States: Implications for Particulate Matter Air Quality. Environmental Science & Technology, 51(20), 11731–11741. https://doi.org/10.1021/acs.est.7b03292

Kebabian, P. L., Herndon, S. C., & Freedman, A. (2005). Detection of Nitrogen Dioxide by Cavity Attenuated Phase Shift Spectroscopy. Analytical Chemistry, 77(2), 724–728. https://doi.org/10.1021/ac048715y

Kebabian, P. L., Wood, E. C., Herndon, S. C., & Freedman, A. (2008). A Practical Alternative to Chemiluminescence-Based Detection of Nitrogen Dioxide: Cavity Attenuated Phase Shift Spectroscopy. Environmental Science & Technology, 42(16), 6040–6045. https://doi.org/10.1021/es703204j

Koplitz, S., Simon, H., Henderson, B., Liljegren, J., Tonnesen, G., Whitehill, A., & Wells, B. (2021). Changes in Ozone Chemical Sensitivity in the United States from 2007 to 2016. ACS Environmental Au. https://doi.org/10.1021/acsenvironau.1c00029

Kuprov, R., Eatough, D. J., Cruickshank, T., Olson, N., Cropper, P. M., & Hansen, J. C. (2014). Composition and secondary formation of fine particulate matter in the Salt Lake Valley: Winter 2009. Journal of the Air & Waste Management Association, 64(8), 957–969. https://doi.org/10.1080/10962247.2014.903878

Lamsal, L. N., Martin, R. V., van Donkelaar, A., Celarier, E. A., Bucsela, E. J., Boersma, K. F., Dirksen, R., Luo, C., & Wang, Y. (2010). Indirect validation of tropospheric nitrogen dioxide retrieved from the OMI satellite instrument: Insight into the seasonal variation of nitrogen oxides at northern midlatitudes. Journal of Geophysical Research: Atmospheres, 115(D5). https://doi.org/10.1029/2009JD013351

Lindaas, J., Farmer, D. K., Pollack, I. B., Abeleira, A., Flocke, F., Roscioli, R., Herndon, S., & Fischer, E. V. (2017). Changes in ozone and precursors during two aged wildfire smoke events in the Colorado Front Range in summer 2015. Atmospheric Chemistry and Physics, 17(17), 10691–10707. https://doi.org/10.5194/acp-17-10691-2017

Linn, J. (2014). Explaining the Adoption of Diesel Fuel Passenger Cars in Europe. SSRN Electronic Journal. https://doi.org/10.2139/ssrn.2432200

Logan, J. A. (1983). Nitrogen oxides in the troposphere: Global and regional budgets. Journal of Geophysical Research: Oceans, 88(C15), 10785–10807. https://doi.org/10.1029/JC088iC15p10785

Lu, X., Zhang, L., & Shen, L. (2019). Meteorology and Climate Influences on Tropospheric Ozone: A Review of Natural Sources, Chemistry, and Transport Patterns. Current Pollution Reports, 5(4), 238–260. https://doi.org/10.1007/s40726-019-00118-3

Ma, S., Tong, D., Harkins, C., McDonald, B. C., Wang, C.-T., Li, Y., Baek, B. H., Woo, J.-H., & Zhang, Y. (2024). Impacts of On-Road Vehicular Emissions on U.S. Air Quality: A Comparison of Two Mobile Emission Models (MOVES and FIVE). Journal of Geophysical Research: Atmospheres, 129(20), e2024JD041494. https://doi.org/10.1029/2024JD041494

Marr, L. C., & Harley, R. A. (2002). Modeling the Effect of Weekday−Weekend Differences in Motor Vehicle Emissions on Photochemical Air Pollution in Central California. Environmental Science & Technology, 36(19), 4099–4106. https://doi.org/10.1021/es020629x

McCarthy, J. E., & Shouse, K. C. (2015). Implementing EPA's 2015 Ozone Air Quality Standards.

McGrath, J. M., Betzelberger, A. M., Wang, S., Shook, E., Zhu, X.-G., Long, S. P., & Ainsworth, E. A. (2015). An analysis of ozone damage to historical maize and soybean yields in the United States. Proceedings of the National Academy of Sciences, 112(46), 14390–14395. https://doi.org/10.1073/pnas.1509777112

Mendoza, D. L., Crosman, E. T., Mitchell, L. E., Jacques, A. A., Fasoli, B., Park, A. M., Lin, J. C., & Horel, J. D. (2019). The TRAX Light-Rail Train Air Quality Observation Project. Urban Science, 3(4), 108. https://doi.org/10.3390/urbansci3040108

Minoura, H., & Ito, A. (2010). Observation of the primary NO2 and NO oxidation near the trunk road in Tokyo. Atmospheric Environment, 44(1), 23–29. https://doi.org/10.1016/j.atmosenv.2009.10.003

Monks, P. S., Archibald, A. T., Colette, A., Cooper, O., Coyle, M., Derwent, R., Fowler, D., Granier, C., Law, K. S., Mills, G. E., Stevenson, D. S., Tarasova, O., Thouret, V., von Schneidemesser, E., Sommariva, R., Wild, O., & Williams, M. L. (2015). Tropospheric ozone and its precursors from the urban to the global scale from air quality to short-lived climate forcer. Atmospheric Chemistry and Physics, 15(15), 8889–8973. https://doi.org/10.5194/acp-15-8889-2015

Mouat, A. P., Siegel, Z. A., & Kaiser, J. (2024). Evaluation of Aeris mid-infrared absorption (MIRA), Picarro CRDS (cavity ring-down spectroscopy) G2307, and dinitrophenylhydrazine (DNPH)-based sampling for long-term formaldehyde monitoring efforts. Atmospheric Measurement Techniques, 17(7), 1979–1994. https://doi.org/10.5194/amt-17-1979-2024

Murphy, J. G., Day, D. A., Cleary, P. A., Wooldridge, P. J., Millet, D. B., Goldstein, A. H., & Cohen, R. C. (2007). The weekend effect within and downwind of Sacramento – Part 1: Observations of ozone, nitrogen oxides, and VOC reactivity. Atmospheric Chemistry and Physics, 7(20), 5327–5339. https://doi.org/10.5194/acp-7-5327-2007

Ninneman, M., Lyman, S., Hu, L., Cope, E., Ketcherside, D., & Jaffe, D. (2023). Investigation of Ozone Formation Chemistry during the Salt Lake Regional Smoke, Ozone, and Aerosol

Study (SAMOZA). ACS Earth and Space Chemistry, 7(12), 2521–2534. https://doi.org/10.1021/acsearthspacechem.3c00235

Nuvolone, D., Petri, D., & Voller, F. (2018). The effects of ozone on human health. Environmental Science and Pollution Research, 25(9), 8074–8088. https://doi.org/10.1007/s11356-017-9239-3

Permar, W., Wang, Q., Selimovic, V., Wielgasz, C., Yokelson, R. J., Hornbrook, R. S., Hills, A. J., Apel, E. C., Ku, I.-T., Zhou, Y., Sive, B. C., Sullivan, A. P., Collett Jr, J. L., Campos, T. L., Palm, B. B., Peng, Q., Thornton, J. A., Garofalo, L. A., Farmer, D. K., … Hu, L. (2021). Emissions of Trace Organic Gases From Western U.S. Wildfires Based on WE-CAN Aircraft Measurements. Journal of Geophysical Research: Atmospheres, 126(11), e2020JD033838. https://doi.org/10.1029/2020JD033838

Pollack, I. B., Helmig, D., O'Dell, K., & Fischer, E. V. (2021). Weekend-Weekday Implications and the Impact of Wildfire Smoke on Ozone and Its Precursors at Boulder Reservoir, Colorado Between 2017 and 2019. Journal of Geophysical Research: Atmospheres, 126(17), e2021JD035221. https://doi.org/10.1029/2021JD035221

Pollack, I. B., Ryerson, T. B., Trainer, M., Parrish, D. D., Andrews, A. E., Atlas, E. L., Blake, D. R., Brown, S. S., Commane, R., Daube, B. C., de Gouw, J. A., Dubé, W. P., Flynn, J., Frost, G. J., Gilman, J. B., Grossberg, N., Holloway, J. S., Kofler, J., Kort, E. A., … Xiang, B. (2012). Airborne and ground-based observations of a weekend effect in ozone, precursors, and oxidation products in the California South Coast Air Basin. Journal of Geophysical Research: Atmospheres, 117(D21). https://doi.org/10.1029/2011JD016772

Pusede, S. E., & Cohen, R. C. (2012). On the observed response of ozone to NOx and VOC reactivity reductions in San Joaquin Valley California 1995–present. Atmospheric Chemistry and Physics, 12(18), 8323–8339. https://doi.org/10.5194/acp-12-8323-2012

Richmond-Bryant, J., Chris Owen, R., Graham, S., Snyder, M., McDow, S., Oakes, M., & Kimbrough, S. (2017). Estimation of on-road NO2 concentrations, NO2/NOX ratios, and related roadway gradients from near-road monitoring data. Air Quality, Atmosphere & Health, 10(5), 611–625. https://doi.org/10.1007/s11869-016-0455-7

Rickly, P. S., Coggon, M. M., Aikin, K. C., Alvarez, R. J. I., Baidar, S., Gilman, J. B., Gkatzelis, G. I., Harkins, C., He, J., Lamplugh, A., Langford, A. O., McDonald, B. C., Peischl, J., Robinson, M. A., Rollins, A. W., Schwantes, R. H., Senff, C. J., Warneke, C., & Brown, S. S. (2023). Influence of Wildfire on Urban Ozone: An Observationally Constrained Box Modeling Study at a Site in the Colorado Front Range. Environmental Science & Technology, 57(3), 1257–1267. https://doi.org/10.1021/acs.est.2c06157

Shindell, D., Faluvegi, G., Lacis, A., Hansen, J., Ruedy, R., & Aguilar, E. (2006). Role of tropospheric ozone increases in 20th-century climate change. Journal of Geophysical Research: Atmospheres, 111(D8). https://doi.org/10.1029/2005JD006348

Shon, Z.-H., Kim, K.-H., & Song, S.-K. (2011). Long-term trend in NO2 and NOx levels and their emission ratio in relation to road traffic activities in East Asia. Atmospheric Environment, 45(18), 3120–3131. https://doi.org/10.1016/j.atmosenv.2011.03.009

Simon, H., Hogrefe, C., Whitehill, A., Foley, K. M., Liljegren, J., Possiel, N., Wells, B., Henderson, B. H., Valin, L. C., Tonnesen, G., Appel, K. W., & Koplitz, S. (2024a). Revisiting day-of-week ozone patterns in an era of evolving US air quality. Atmospheric Chemistry and Physics, 24(3), 1855–1871. https://doi.org/10.5194/acp-24-1855-2024

Simon, H., Hogrefe, C., Whitehill, A., Foley, K. M., Liljegren, J., Possiel, N., Wells, B., Henderson, B. H., Valin, L. C., Tonnesen, G., Appel, K. W., & Koplitz, S. (2024b). Revisiting day-of-week ozone patterns in an era of evolving US air quality. Atmospheric Chemistry and Physics, 24(3), 1855–1871. https://doi.org/10.5194/acp-24-1855-2024

Smith, H. (2021, August 25). Smoke from Northern California's wildfires is moving toward Los Angeles. Los Angeles Times. https://www.latimes.com/california/story/2021-08-25/smoke-northern-california-wildfires-moving-toward-los-angeles

Stavrakou, T., Müller, J.-F., Bauwens, M., Boersma, K. F., & van Geffen, J. (2020). Satellite evidence for changes in the NO2 weekly cycle over large cities. Scientific Reports, 10(1), 10066. https://doi.org/10.1038/s41598-020-66891-0

Tian, L., Hossain, S. R., Lin, H., Ho, K. F., Lee, S. C., & Yu, I. T. S. (2011). Increasing trend of primary NO2 exhaust emission fraction in Hong Kong. Environmental Geochemistry and Health, 33(6), 623–630. https://doi.org/10.1007/s10653-011-9375-5

Tillmann, R., Gkatzelis, G. I., Rohrer, F., Winter, B., Wesolek, C., Schuldt, T., Lange, A. C., Franke, P., Friese, E., Decker, M., Wegener, R., Hundt, M., Aseev, O., & Kiendler-Scharr, A. (2022). Air quality observations onboard commercial and targeted Zeppelin flights in Germany – a platform for high-resolution trace-gas and aerosol measurements within the planetary boundary layer. Atmospheric Measurement Techniques, 15(12), 3827–3842. https://doi.org/10.5194/amt-15-3827-2022

Tilton, B. E. (1989). Health effects of tropospheric ozone. Environmental Science & Technology, 23(3), 257–263. https://doi.org/10.1021/es00180a002

UDAQ. (2025). Network Review—Air Monitoring Program—Utah Department of Environmental Quality. https://air.utah.gov/

UDEQ. (2024). Utah Air Monitoring Program. https://air.utah.gov/

US EPA, O. (2015a, June 5). Health Effects of Ozone Pollution [Overviews and Factsheets]. https://www.epa.gov/ground-level-ozone-pollution/health-effects-ozone-pollution

US EPA, O. (2015b, June 11). Ecosystem Effects of Ozone Pollution [Overviews and Factsheets]. https://www.epa.gov/ground-level-ozone-pollution/ecosystem-effects-ozone-pollution

US EPA, O. (2015c, July 27). Air Pollutant Emissions Trends Data [Other Policies and Guidance]. https://www.epa.gov/air-emissions-inventories/air-pollutant-emissions-trends-data

US EPA, O. (2020). 2020 National Emissions Inventory (NEI) Data [Other Policies and Guidance]. https://www.epa.gov/air-emissions-inventories/2020-national-emissions-inventory-nei-data

US EPA, O. (2025). NAAQS Table [Other Policies and Guidance]. https://www.epa.gov/criteria-air-pollutants/naaqs-table

Valin, L. C., Russell, A. R., & Cohen, R. C. (2014). Chemical feedback effects on the spatial patterns of the NOx weekend effect: A sensitivity analysis. Atmospheric Chemistry and Physics, 14(1), 1–9. https://doi.org/10.5194/acp-14-1-2014

Wang, X., Cai, Y., Wang, J., & Zhao, Y. (2021). Concentration monitoring of volatile organic compounds and ozone in Xi'an based on PTR-TOF-MS and differential absorption lidar. Atmospheric Environment, 245, 118045. https://doi.org/10.1016/j.atmosenv.2020.118045

Wang, Y., Liu, P., Schwartz, J., Castro, E., Wang, W., Chang, H., Scovronick, N., & Shi, L. (2023). Disparities in ambient nitrogen dioxide pollution in the United States. Proceedings of the National Academy of Sciences, 120(16), e2208450120. https://doi.org/10.1073/pnas.2208450120

Wild, R. J., Dubé, W. P., Aikin, K. C., Eilerman, S. J., Neuman, J. A., Peischl, J., Ryerson, T. B., & Brown, S. S. (2017). On-road measurements of vehicle NO2/NOx emission ratios in Denver, Colorado, USA. Atmospheric Environment, 148, 182–189. https://doi.org/10.1016/j.atmosenv.2016.10.039

Xiang, S., Zhang, S., Wang, H., Yu, Y. T., Wallington, T. J., Shen, W., Kirchner, U., Deng, Y., Tan, Q., Zhou, Z., & Wu, Y. (2022). Variability of NO2/NOx Ratios in Multiple Microenvironments from On-Road and Near-Roadway Measurements. ACS ES&T Engineering, 2(9), 1599–1610. https://doi.org/10.1021/acsestengg.2c00027

Xu, L., Crounse, J. D., Vasquez, K. T., Allen, H., Wennberg, P. O., Bourgeois, I., Brown, S. S., Campuzano-Jost, P., Coggon, M. M., Crawford, J. H., DiGangi, J. P., Diskin, G. S., Fried, A., Gargulinski, E. M., Gilman, J. B., Gkatzelis, G. I., Guo, H., Hair, J. W., Hall, S. R., … Yokelson, R. J. (2021). Ozone chemistry in western U.S. wildfire plumes. Science Advances, 7(50), eabl3648. https://doi.org/10.1126/sciadv.abl3648

Yañez, C. C., Bares, R., Czimczik, C. I., Lin, J., Zhang, J., Bush, S., & Hopkins, F. M. (2025). Contrasting Summertime Trends in Vehicle Combustion Efficiency in Los Angeles, CA and Salt Lake City, UT. Environmental Science & Technology, 59(2), 1287–1297. https://doi.org/10.1021/acs.est.4c11701

Zetlen, H. L., Rifas-Shiman, S. L., Gibson, H., Oken, E., Gold, D. R., & Rice, M. B. (2025). Long-Term Exposure to Nitrogen Dioxide and Ozone and Respiratory Health in Children. Annals of the American Thoracic Society. https://doi.org/10.1513/AnnalsATS.202405-455OC

Zuraski, K., Harkins, C., Peischl, J., Coggon, M. M., Stockwell, C. E., Robinson, M. A., Gilman, J., Warneke, C., McDonald, B. C., & Brown, S. S. (2025). On-Road Measurements of

Nitrogen Oxides, CO, CO2, and VOC Emissions in Two Southwestern U.S. Cities. ACS ES&T Air, 2(4), 589–598. https://doi.org/10.1021/acsestair.4c00316

APPENDIX: SUPPLEMENTAL FIGURES

I. SLC-SOS Driving Schedule

Figure A1. SLC-SOS field campaign color-coded driving schedule. Green squares represent mobile drive sampling days, sky-blue squares indicate stationary sampling, orange shows calibration days, and yellow the down days. Each box includes the drive day (e.g., D1, D2) and the corresponding driving locations. The campaign began with transit to Salt Lake City, UT on May 30, 2024, and concluded with return transit to Laramie, WY on June 30, 2024.

II. SLC-SOS Payload

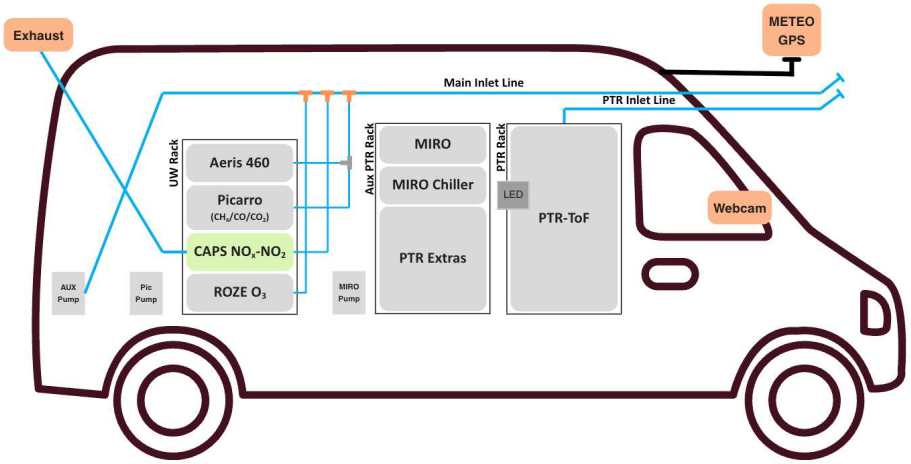

Figure A2. UWyo Mobile Research Laboratory deployment schematic showing the configuration of the inlet and exhaust lines, Monitoring System (AIO), GPS, webcam, pumps, and the locations of various instruments inside the vehicle. Instruments include: Aeris 460, Picarro, CAPS NO_x-NO_2, ROZE, MIRO, and PTR-ToF-MS.

III. CAPS NO_x-NO_2 Instrument

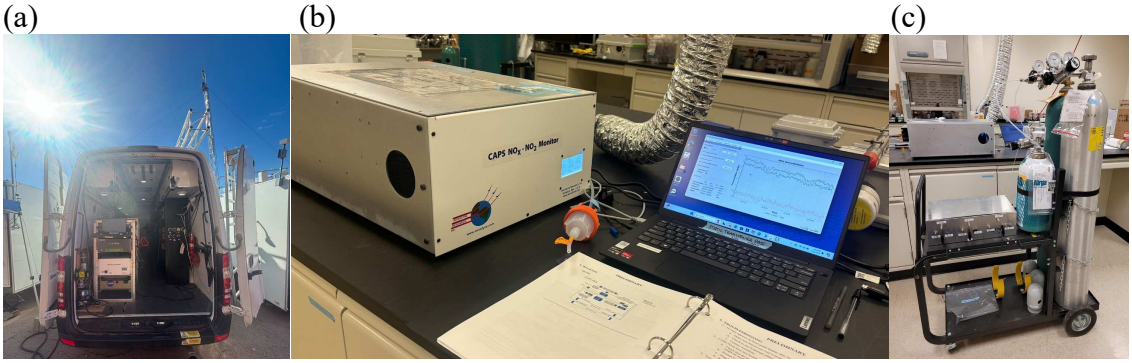

Figure A3. (a) UWyom Mobile Research Laboratory back view. (b) CAPS NO_X-NO_2 Monitor. (c) CAPS NO_x-NO_2 Cal-Cart.

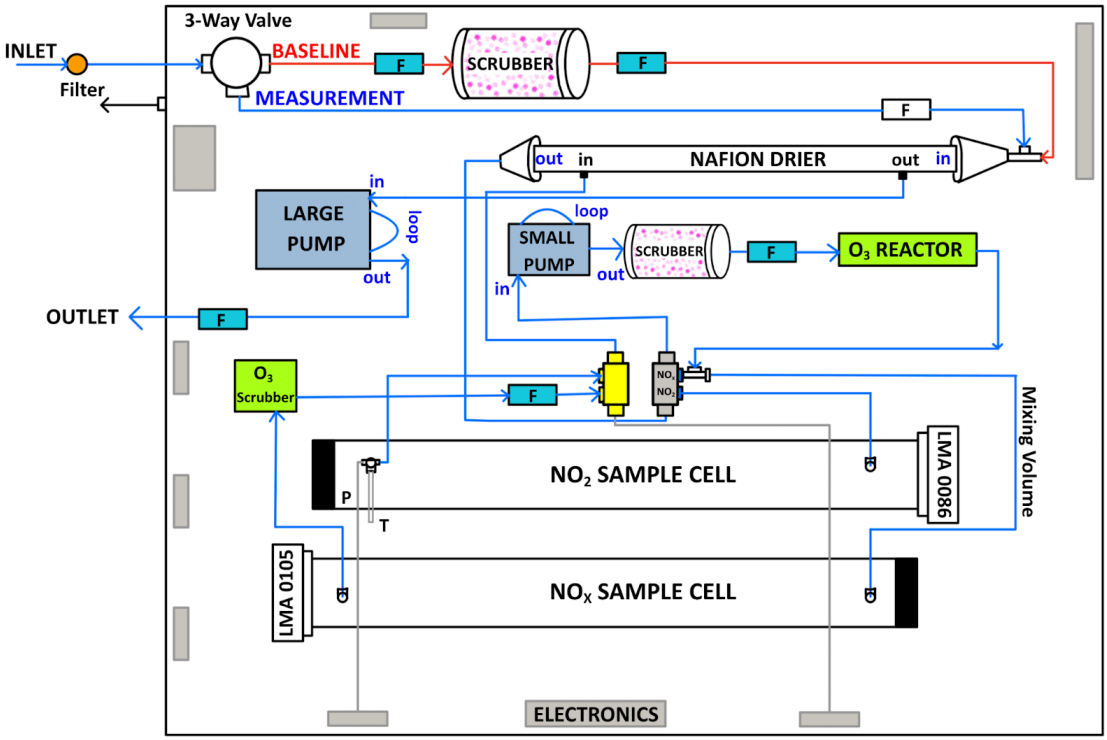

Figure A4. Schematic of the CAPS NO_x-NO_2 Monitor.

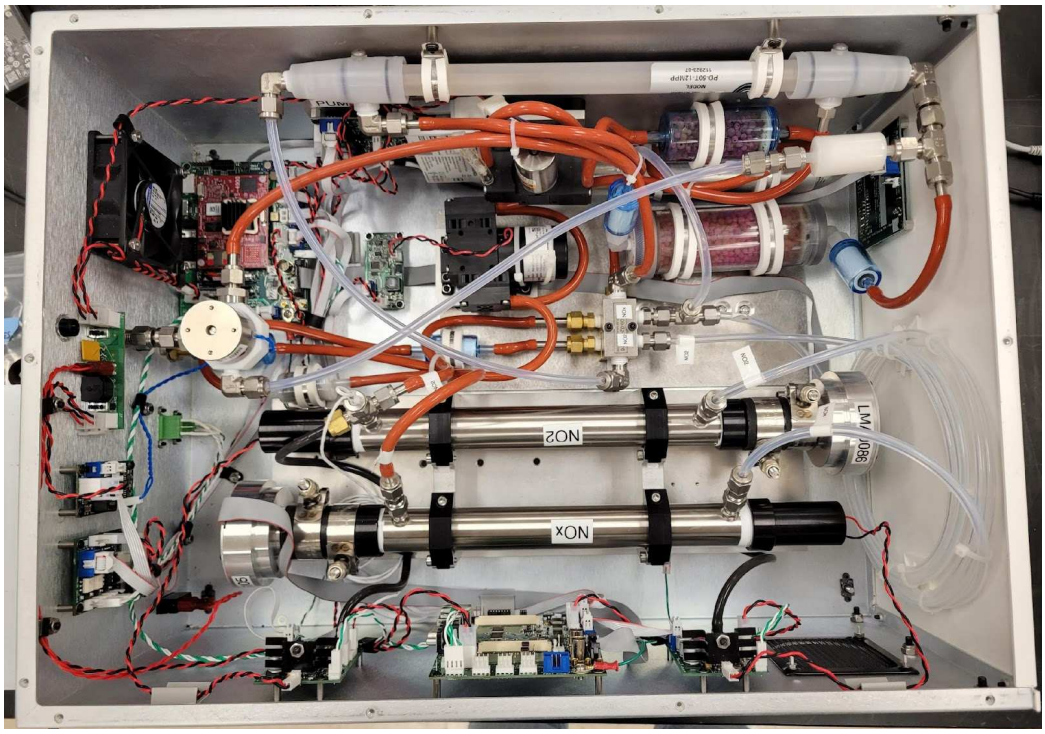

Figure A5. Inside the CAPS NO_x-NO_2 Instrument Box.

IV. CAPS NO_x-NO_2 Uncertainties and Calibrations

A. Uncertainties in mixing ratios

Using the equation of Uncertainty in Sums and Differences (Eq. 1) from the Book: "Error Analysis" from John Taylor, Chapter 3. Suppose that x,..., w are measured with uncertainties δx, …, δw and the measured values used to compute:

$$q = x + \cdots + z - (u + \cdots + w)$$

If the uncertainties in x, …, w are known to be independent and random, then the uncertainty in q is the quadratic sum of the original uncertainties:

$$Total = \delta q = \sqrt{(\delta x)^2 + \cdots + (\delta z)^2 + (\delta u)^2 + \cdots + (\delta w)^2} \qquad \text{(Eq.1)}$$

where δq is never larger than their ordinary sum,

$$\delta q \leq \delta x + \cdots + \delta z + \delta u + \cdots + \delta w$$

- Calibration Gas Flow, CalCart/DryCals: $\pm$ 0.5% $uncertainty = 5\ x10^{-3}$
- Sample Flow, DryCals: $\pm$ 0.5% $unceratinty = 5\ x\ 10^{-3}$
- Mixing Ratio, Gas Standards:
    - NO: $1.07\ \pm 0.10\ ppm\ NO\ in\ NO_2$

      NO: $\frac{0.10\ ppm}{1.07\ ppm} = 0.0934\ x\ 100\% = 9.346\ \%\ uncertainty$
    - NO_2: $1.164\ \pm 0.116\ ppm$

      NO_2: $\frac{0.116\ ppm}{1.164\ ppm} = 0.0997\ x\ 100\% = 9.966\%\ uncertainty$

$$NO\ Total = \sqrt{(5\ x\ 10^{-3})^2 + (5\ x\ 10^{-3})^2 + (0.0934)^2} = 0.0937 = 9.367\ \% \simeq 10\%$$

$$NO_2 Total = \sqrt{(5\ x\ 10^{-3})^2 + (5\ x\ 10^{-3})^2 + (0.0997)^2} = 0.0999 = 9.995\ \% \simeq 10\%$$

B. Calibrations

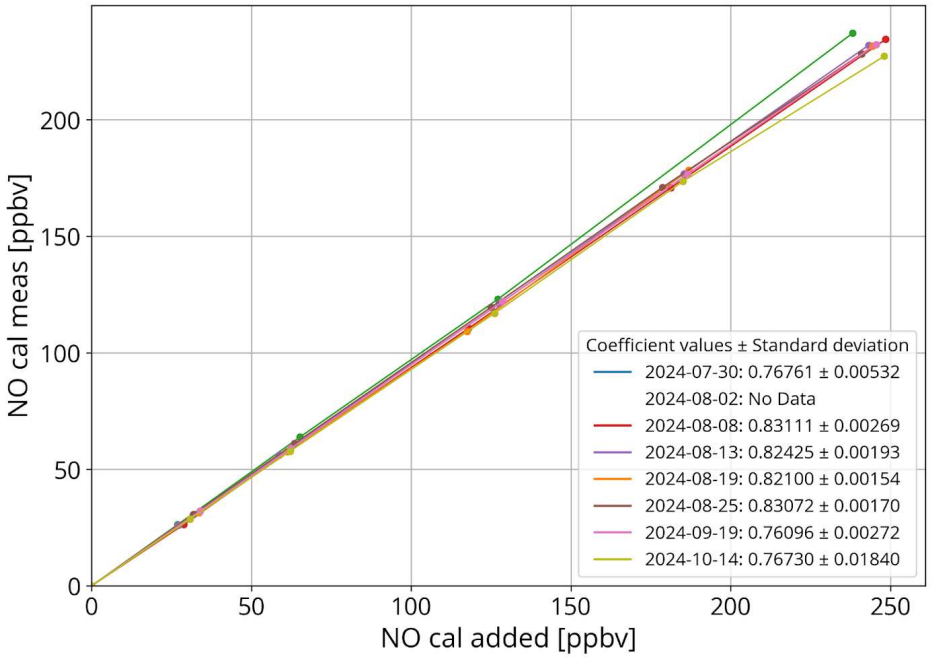

Figure A6. NO calibration curves.

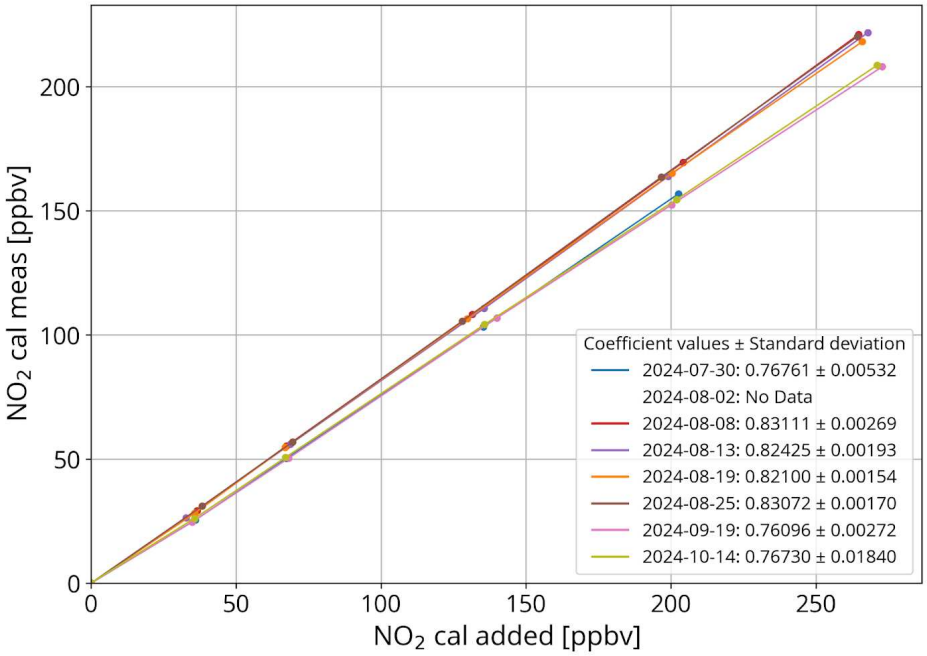

Figure A7. NO_2 calibration curves.

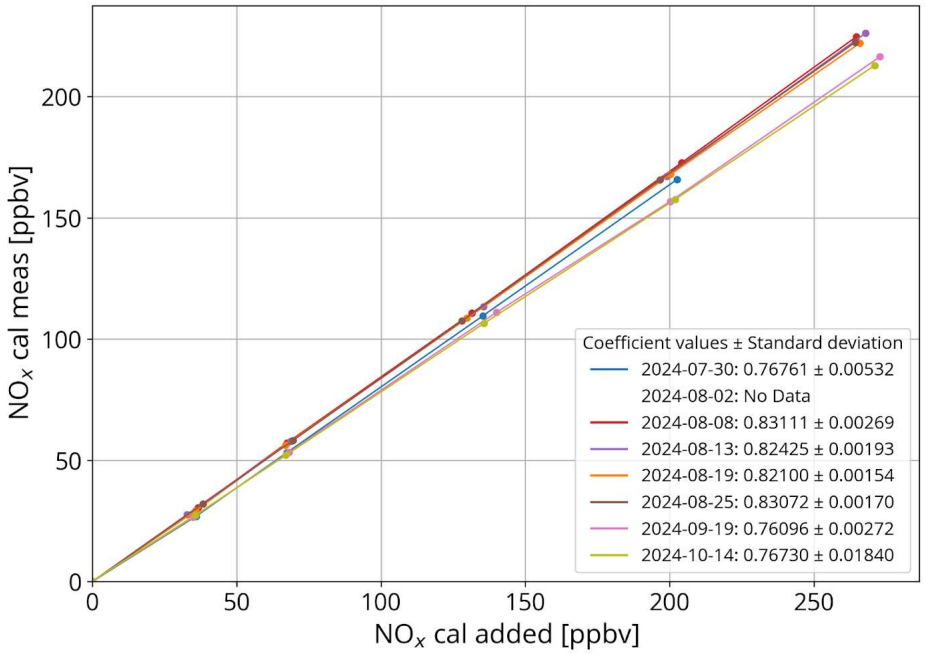

Figure A8. NO_x calibration curves.

V. NO_2/NO_x Ratios

A. Flowcharts

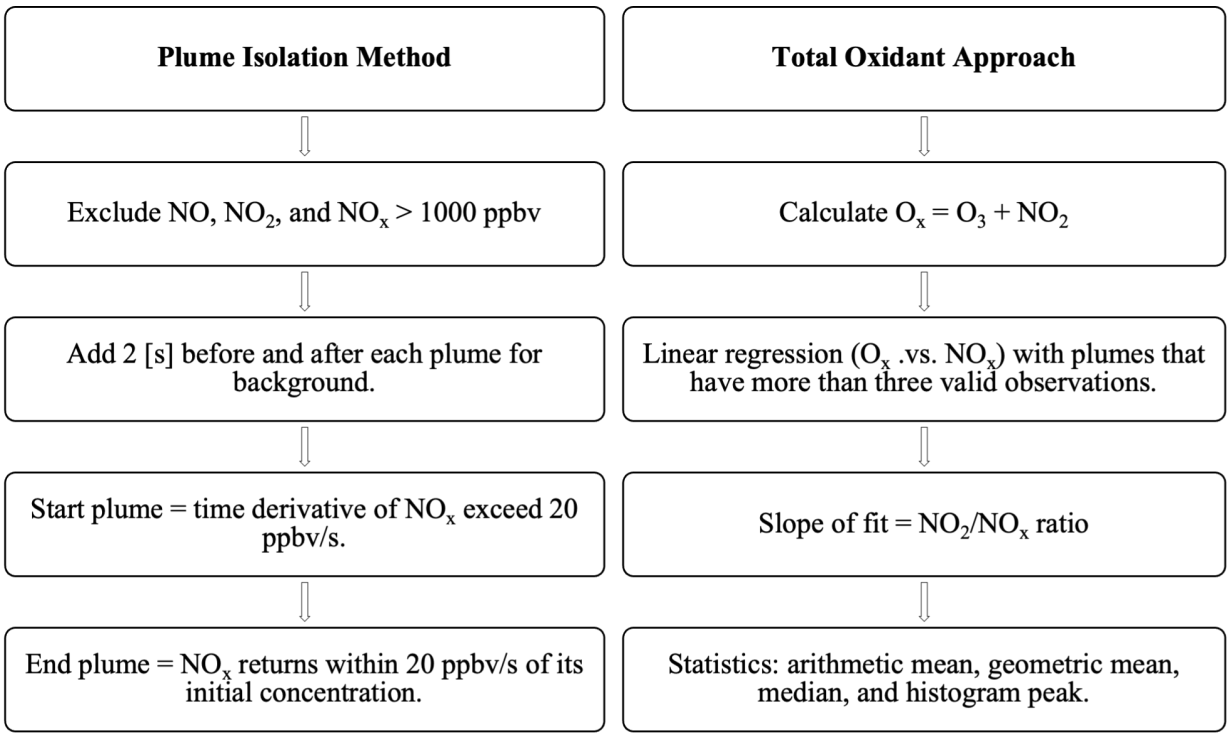

Figure A9. Flowcharts for the plume isolation method and the total oxidant approach.

B. Including negative NO_2/NO_x ratios

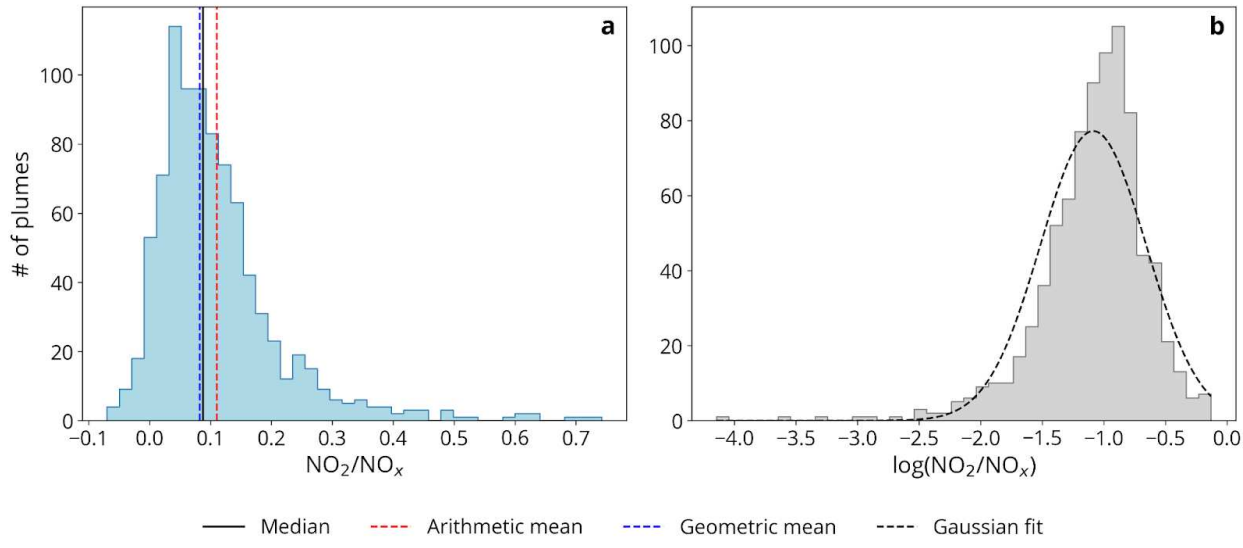

Figure A10. Histogram distribution of NO_2/NO_x ratios for a threshold of 20 ppbv/s.

Salt Lake City, UT	
Total # of plumes	878

Arithmetic mean	0.1106 ± 0.1051
Geometric mean	-
Median	0.0878
Histogram peak	0.0629

Table A1. Statistical values of NO_2/NO_x ratios from smoke-free drives for a threshold of 20 ppbv/s. Negative values are included, except for the geometric mean and in the logarithmic plot.

C. Vehicle speed and air temperature

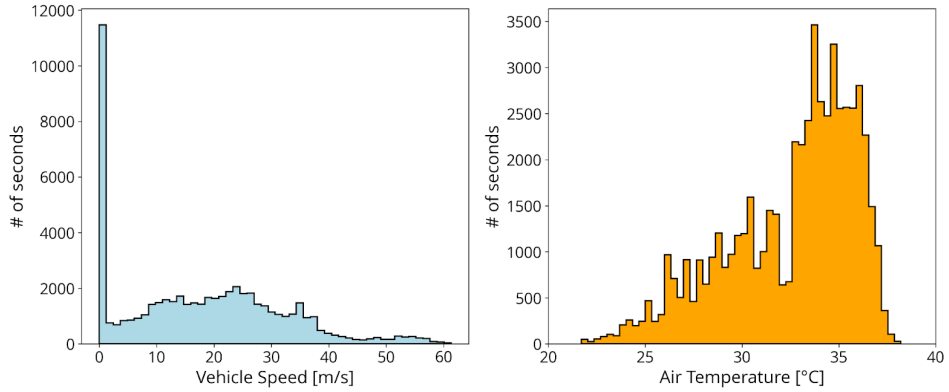

Figure A11. Vehicle speed and air temperature.

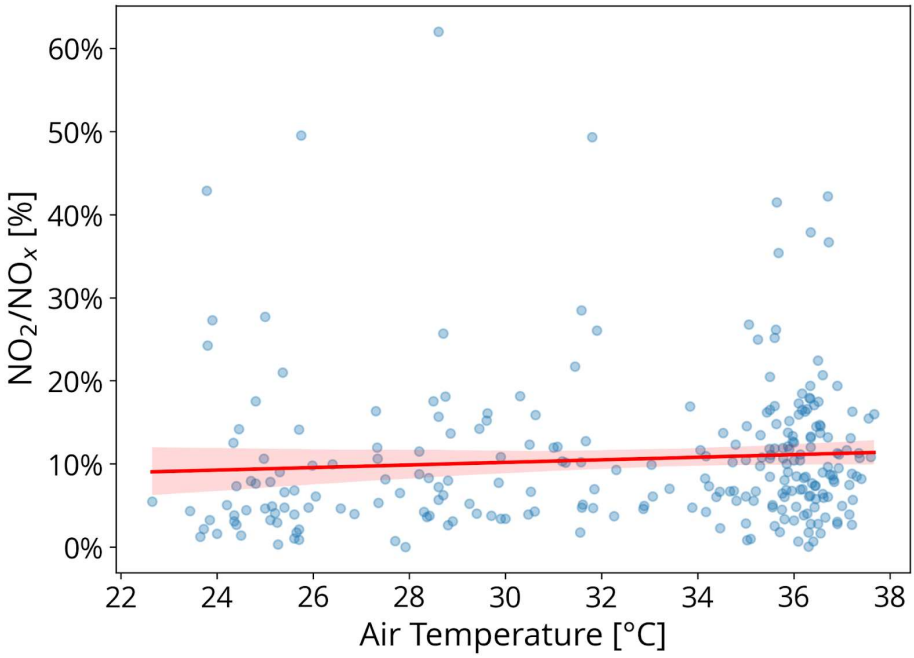

Figure A12. NO_2/NO_x versus air temperature for all plumes identified in smoke-free drives using the 20 ppbv/s threshold.

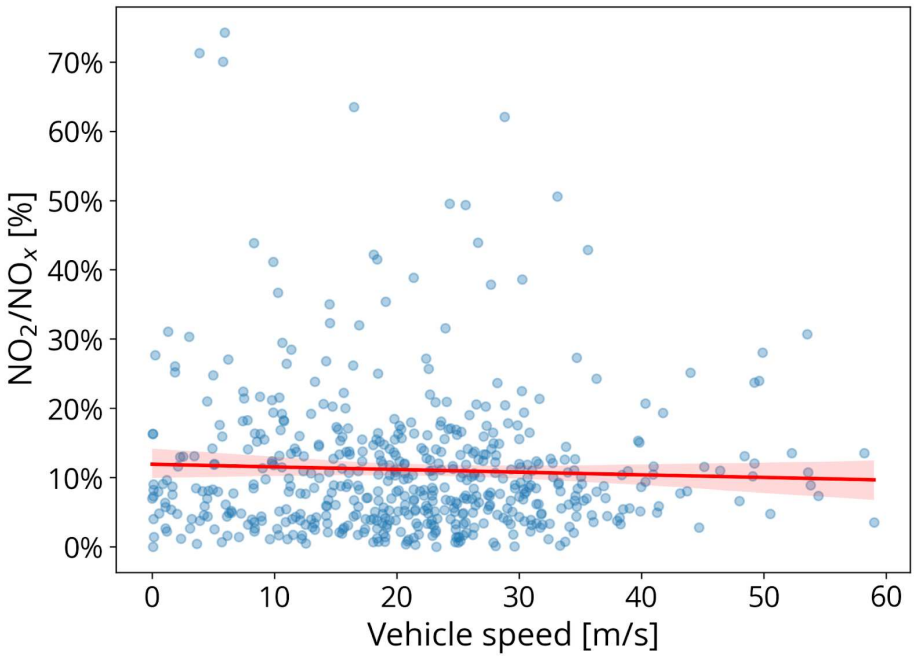

Figure A13. NO_2/NO_x versus vehicle speed for all plumes identified in smoke-free drives using the 20 ppbv/s threshold.

D. Linear regression (O_x and NO_x) for each plume containing more than five valid observations

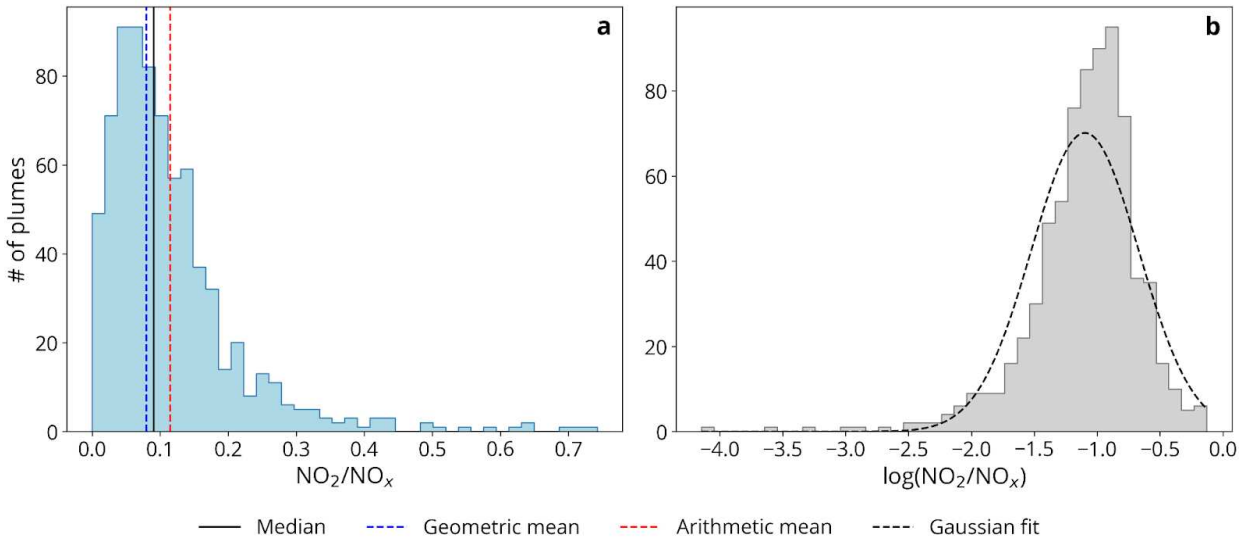

Figure A14. Histogram distribution of NO_2/NO_x ratios for a threshold for the time derivative of NO_x exceeding 20 ppbv/s for each plume containing more than five valid observations.

Salt Lake City, UT	
Total # of plumes	786

Arithmetic mean	0.1147 ± 0.0997
Geometric mean	0.0800 ± 0.9834
Median	0.0909
Histogram peak	0.0655

Table A2. Statistical values of NO_2/NO_x ratios from smoke-free drives for a threshold for the time derivative of NO_x exceeding 20 ppbv/s for each plume containing more than five valid observations.

E. Linear regression (O_x and NO_x) for each plume containing more than five valid observations and $R^2 > 0.6$

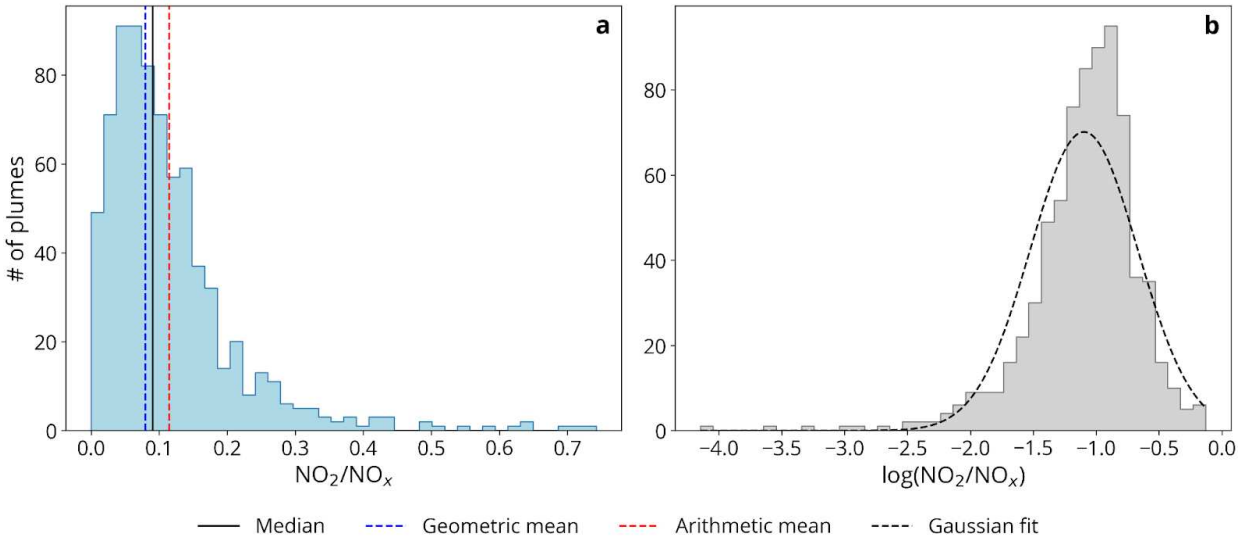

Figure A15. Histogram distribution of NO_2/NO_x ratios for a threshold for the time derivative of NO_x exceeding 20 ppbv/s.

Salt Lake City, UT	
Total # of plumes	285
Arithmetic mean	0.1721 ± 0.1233
Geometric mean	0.1395 ± 0.6534
Median	0.1380
Histogram peak	0.1195

Table A3. Statistical values of NO_2/NO_x ratios from smoke-free drives for a threshold for the time derivative of NO_x exceeding 20 ppbv/s. Negative values are included, except for the geometric mean and in the logarithmic plot.

F. Thresholds of 25 ppbv/s and 30 ppbv/s

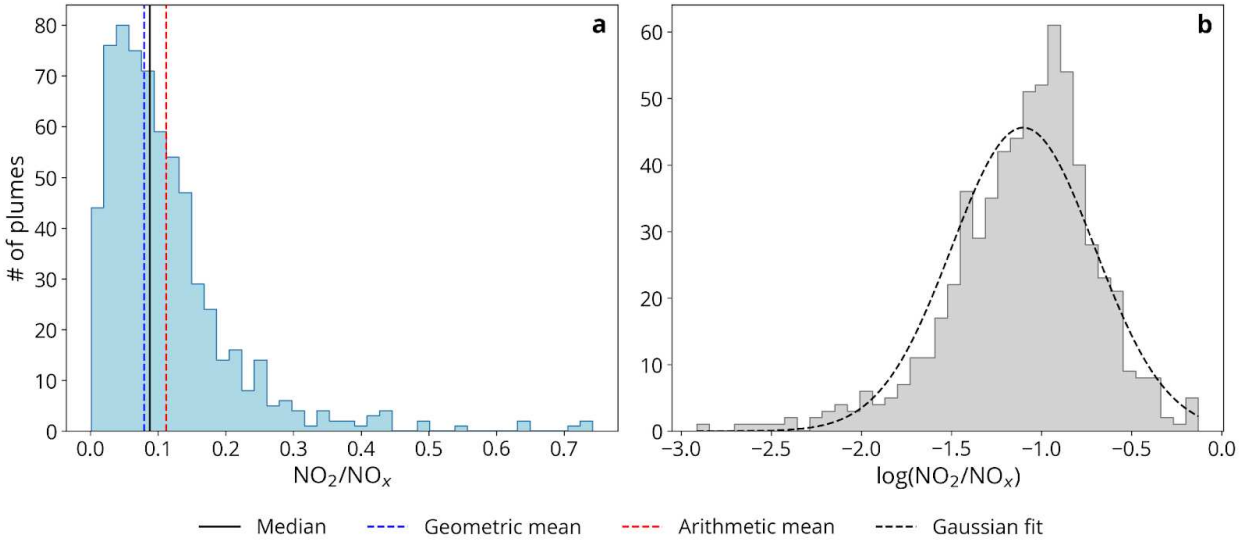

Figure A16. Histogram distribution of NO_2/NO_x ratios for a threshold for the time derivative of NO_x exceeding 25 ppbv/s.

Salt Lake City, UT	
Total # of plumes	685
Arithmetic mean	0.1120 ± 0.0988
Geometric mean	0.0791 ± 0.9124
Median	0.0876
Histogram peak	0.0606

Table A4. Statistical values of NO_2/NO_x ratios from smoke-free drives for a threshold for the time derivative of NO_x exceeding 25 ppbv/s.

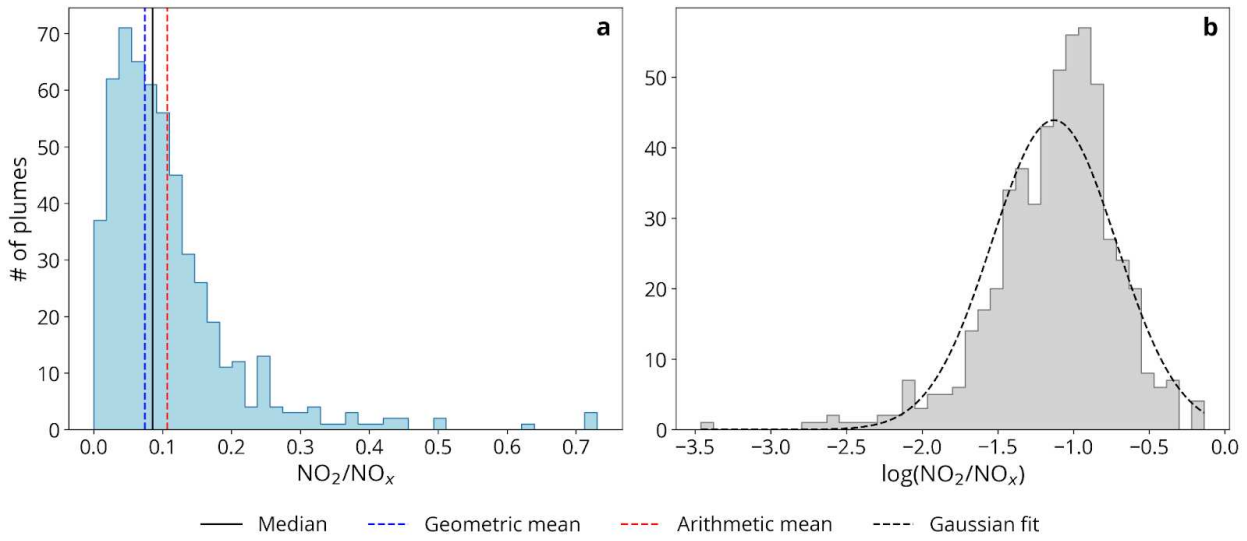

Figure A17. Histogram distribution of NO_2/NO_x ratios for a threshold for the time derivative of NO_x exceeding 30 ppbv/s.

Salt Lake City, UT	
Total # of plumes	572
Arithmetic mean	0.1067 ± 0.0962
Geometric mean	0.0743 ± 0.9457
Median	0.0855
Histogram peak	0.0603

Table A5. Statistical values of NO_2/NO_x ratios from smoke-free drives for a threshold for the time derivative of NO_x exceeding 30 ppbv/s.

VI. Regional NO_x gradients wind patterns

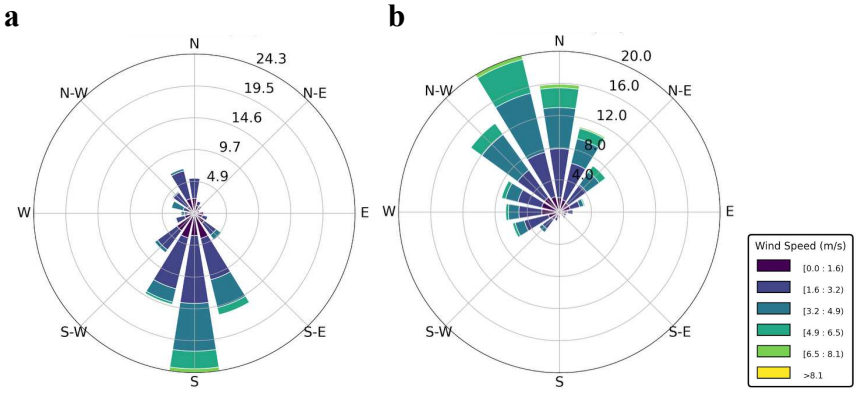

Figure A18. Wind roses for the Lake Breeze route on 21 August 2024. (a) Southerly morning conditions with an average speed of 3.24 m/s; and (b) northwesterly afternoon conditions with an average speed of 3.03 m/s.

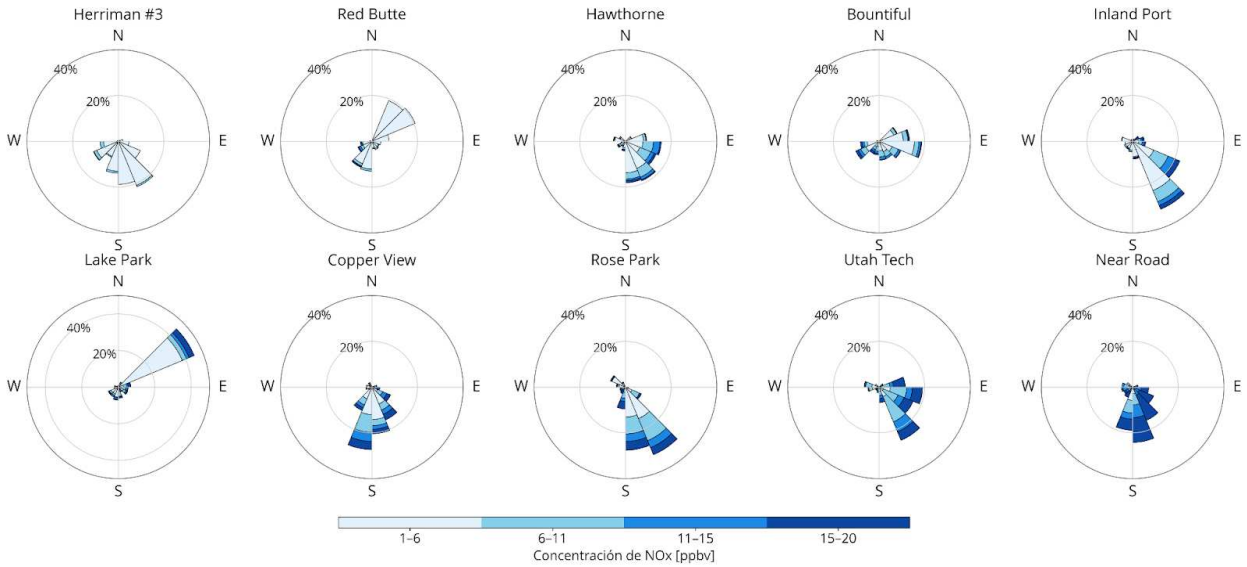

Figure A19. Pollution wind roses of NO_x for smoke-free days at ten DAQ Monitoring Sites during August 2024.

VII. Weekday-Weekend Differences

A. All August (including both smoke-free and smoke-impacted days)

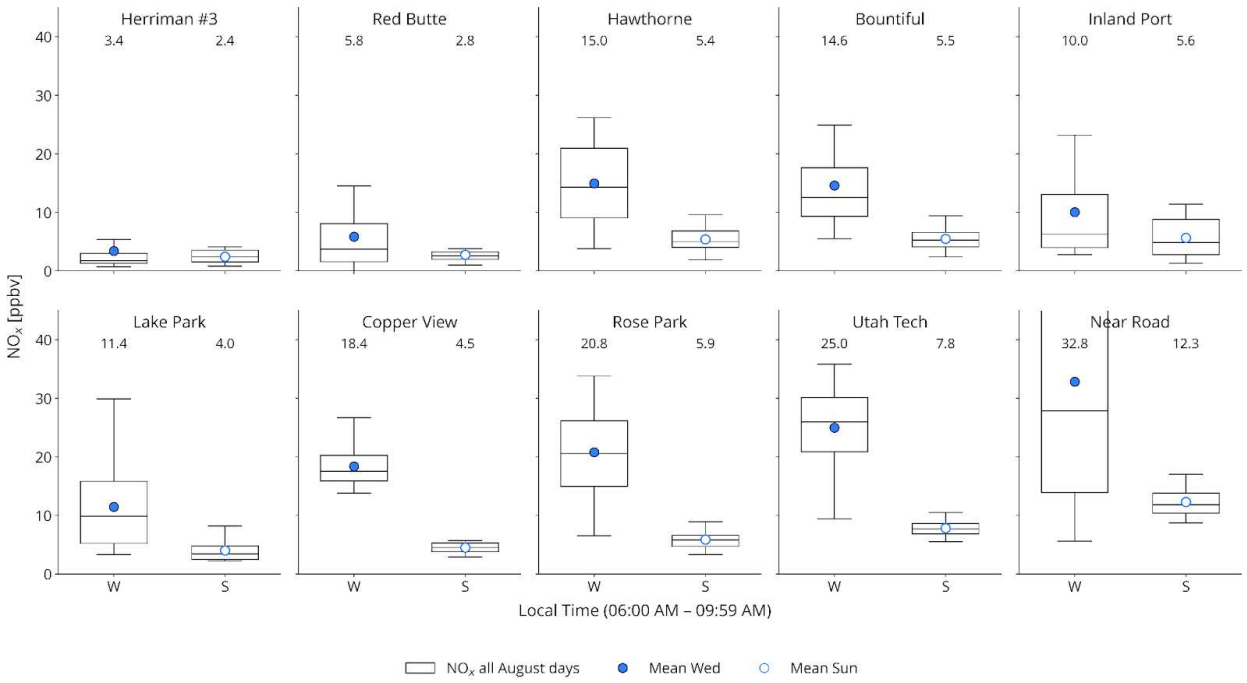

Figure A20. Boxplots of NO_x mixing ratios observed during the morning period (06:00 AM - 09:59 AM) for the ten DAQ monitoring sites during August 2024. Panels follow the same site order as the diurnal profiles. Boxes extend from the 25th to 75th percentile, whiskers extend from the minimum to the maximum values, and the median is indicated by the horizontal line across each

box. Colored circles represent the mean values for Wednesday (solid blue) and Sunday (open blue) and numeric values above each box plot indicate the mean NO_x concentration.

B. All summer (June to September 2024) for Wednesday and Sunday

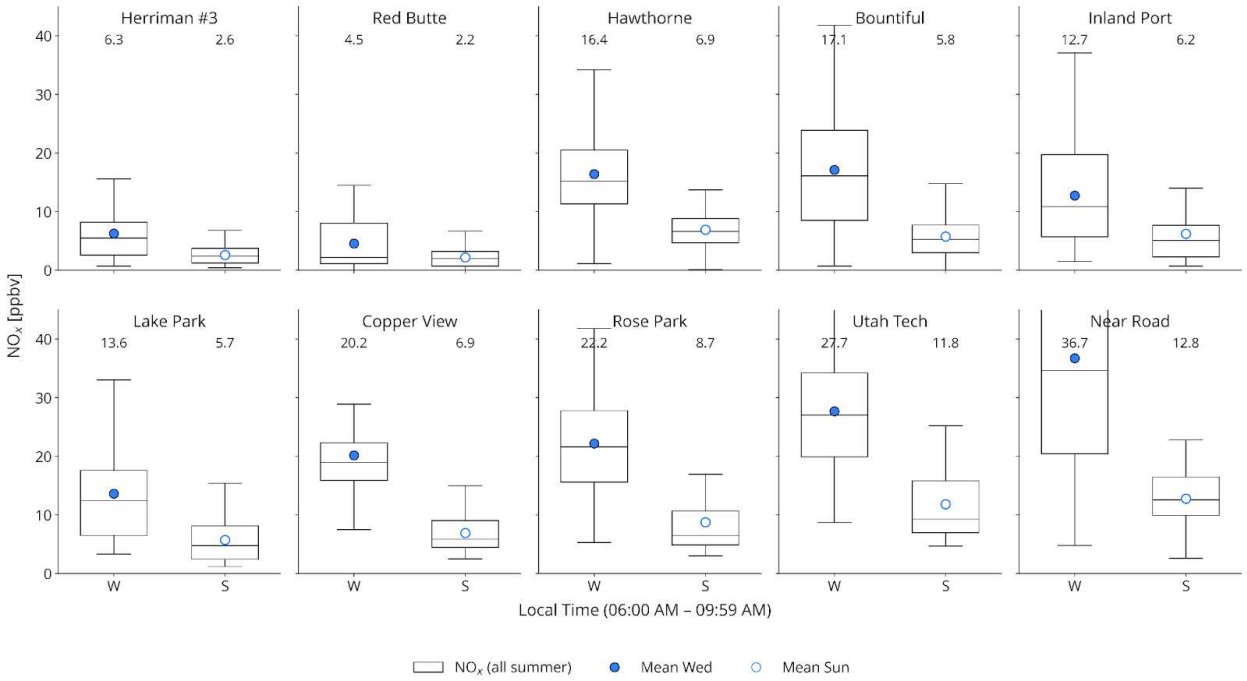

Figure A21. Boxplots of NO_x mixing ratios observed during the morning period (06:00 AM - 09:59 AM) for the ten DAQ monitoring sites during June - September 2024. Panels follow the same site order as the diurnal profiles. Boxes extend from the 25th to 75th percentile, whiskers extend from the minimum to the maximum values, and the median is indicated by the horizontal line across each box. Colored circles represent the mean values for Wednesday (solid blue) and Sunday (open blue) and numeric values above each box plot indicate the mean NO_x concentration.

C. All summer (June to September 2024) for Wednesday and Saturday

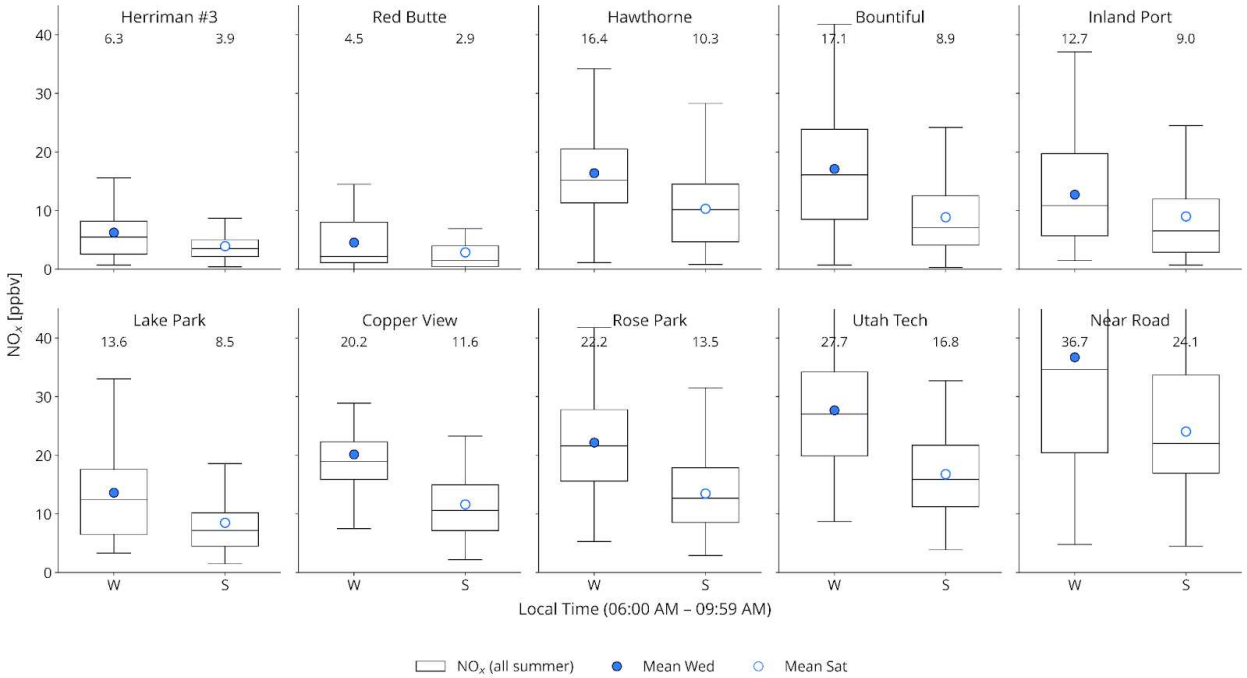

Figure A22. Boxplots of NO_x mixing ratios observed during the morning period (06:00 AM - 09:59 AM) for the ten DAQ monitoring sites during June - September 2024. Panels follow the same site order as the diurnal profiles. Boxes extend from the 25th to 75th percentile, whiskers extend from the minimum to the maximum values, and the median is indicated by the horizontal line across each box. Colored circles represent the mean values for Wednesday (solid blue) and Saturday (open blue) and numeric values above each box plot indicate the mean NO_x concentration.

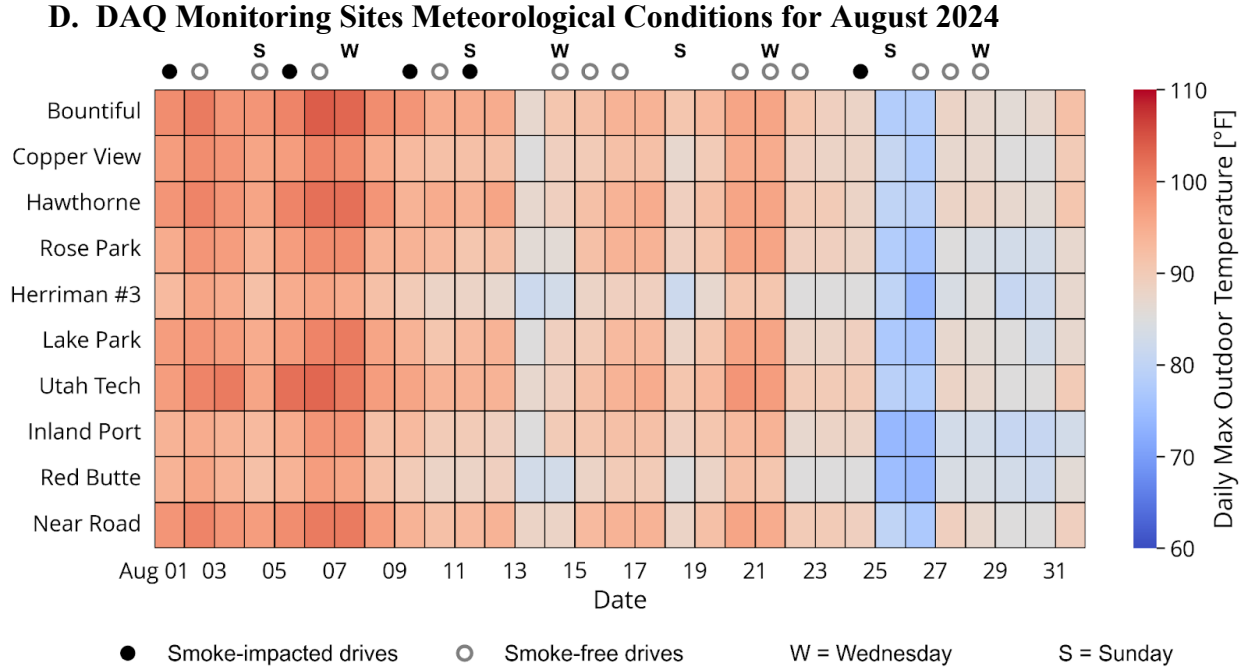

Figure A23. Daily maximum outdoor temperature (°F) across monitoring stations in Salt Lake City during August 2024. Each row represents a monitoring site, and each column corresponds to a day.

Colored circles in the top indicate the smoke influence status of the drives: smoke-free (white) and smoke-impacted (gray). Letters denote day of the week: W = Wednesday and S = Sunday.

VIII. Future Work

A. Smoke-free versus no-smoke differences

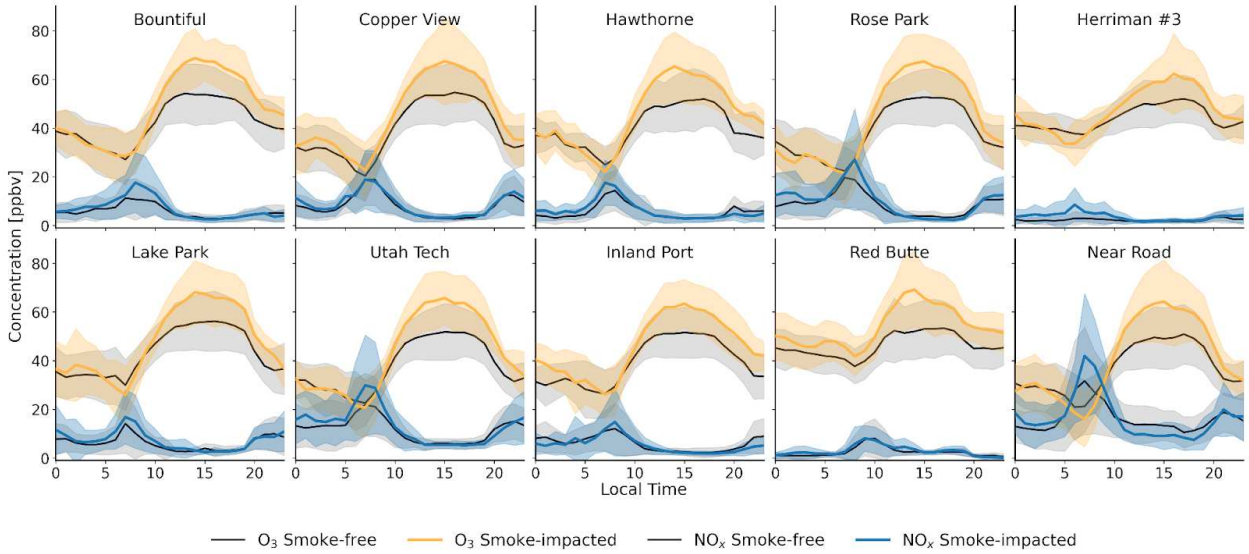

Figure A24. Diurnal profiles of NO, NO_2, and O_3 [ppb] for DAQ Monitoring Sites in MT during August 2024. The lines indicate the mean in 1 hour and the shaded regions around are 1 standard deviation from the mean. Yellow and blue lines correspond to smoke-impacted days while black lines represent smoke-free days.

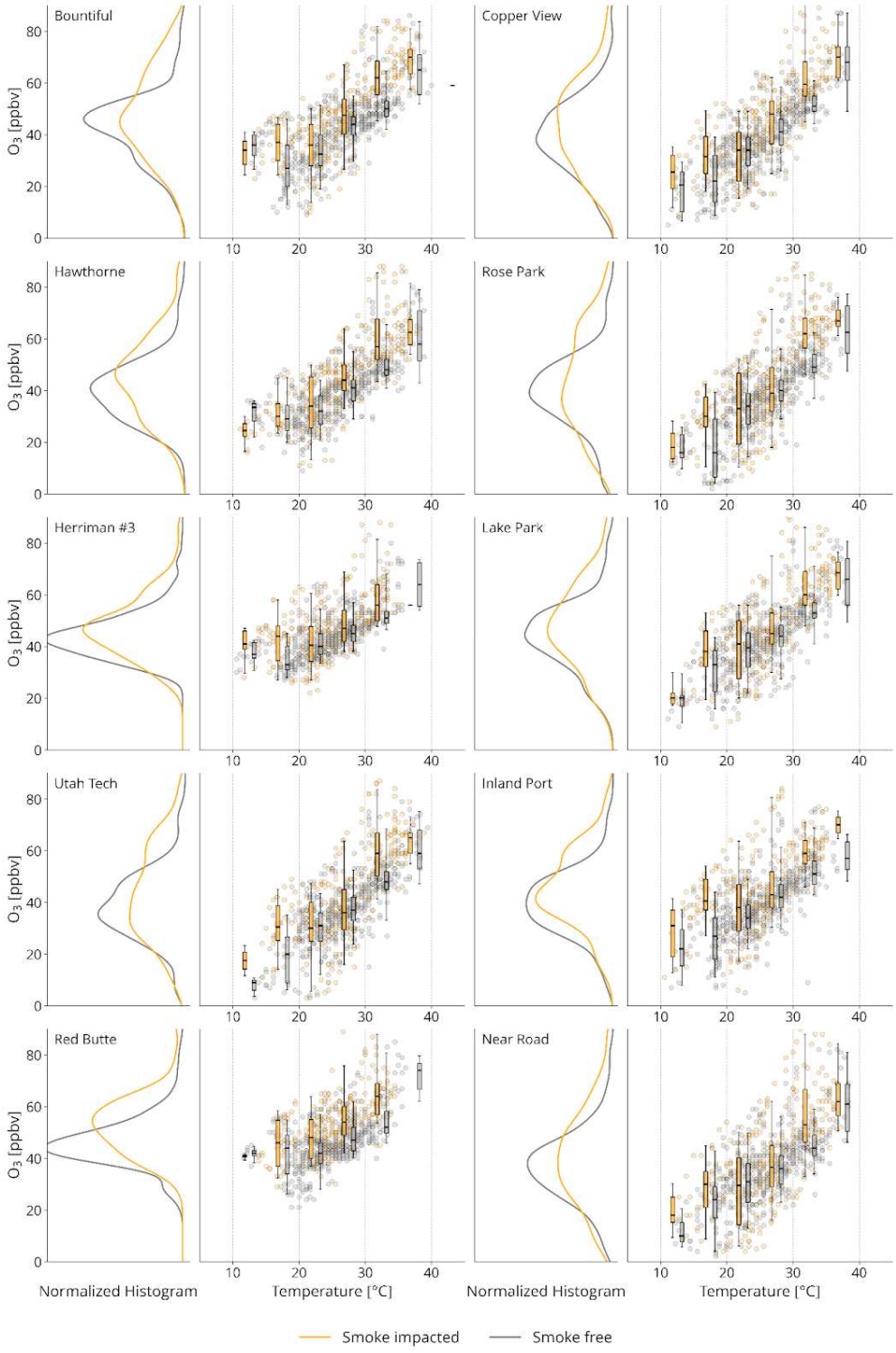

Figure A25. Distribution of hourly O_3 and ambient temperature across DAQ Monitoring Sites during August. (Left) Normalized histograms of O_3 for smoke-free (gray) and smoke-impacted (yellow) conditions. (Right) Scatter plots for O_3 as a function of air temperature and overlaid box plots representing the 5th, 25th, 50th, 75th, and 95th percentiles in 5 °C bins.

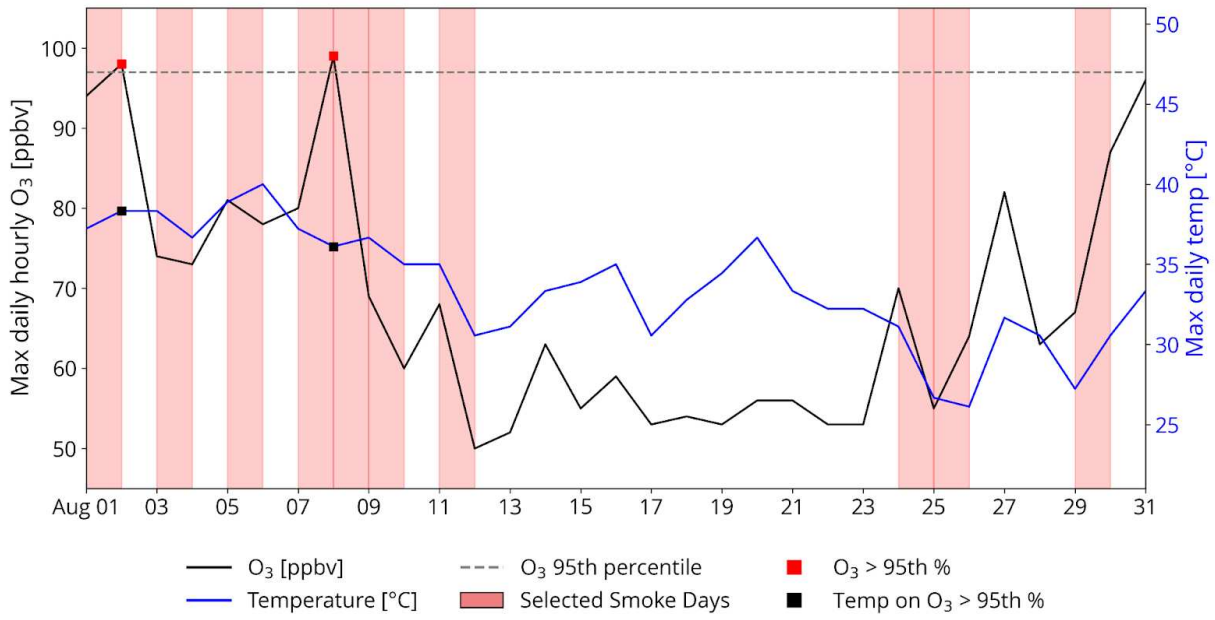

Figure A26. Daily maximum hourly O_3 mixing ratios and daily maximum temperature averaged across DAQ monitoring stations between 10:00 and 18:00 MT in August 2024. Red shaded areas indicate selected smoke days, and the horizontal dashed line shows the 95th percentile of all daily maximum O_3 values. Red squares mark days when O_3 exceeded this threshold, and black squares mark the corresponding daily temperatures on those high O_3 days.